RELOCATION OF EARTHQUAKES IN THE SALT LAKE REGION USING THE HYPOCENTROIDAL DECOMPOSITION (HDC) METHOD

by

Burak Sakarya

B.S., Geophysical Engineering , Kocaeli University, 2012

Submitted to the Kandilli Observatory and Earthquake Research Institute in partial fulfillment of the requirements for the degree of Master of Science

Graduate Program in Geophysics

Boğaziçi University

2017

RELOCATION OF EARTHQUAKES
IN THE SALT LAKE REGION USING THE
HYPOCENTROIDAL DECOMPOSITION (HDC) METHOD

APPROVED BY:

Assoc. Prof. Dr. Ali Özgün Konca ..... 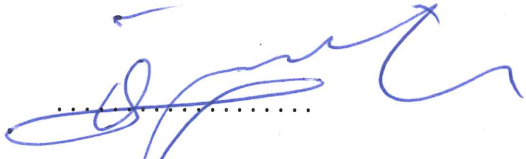
(Thesis Supervisor)

Prof. Dr. Ali Pınar ..... 

Assoc. Prof. Dr. Tahir Serkan Irmak ..... 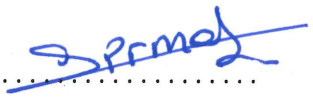
(Kocaeli University)

DATE OF APPROVAL: 08.09.2017

ACKNOWLEDGEMENTS

I would like to express my deep gratitude to Prof. Dr. Niyazi Türkelli, my thesis advisor, for his guidance and persistent help in this masters study. He provided me to attend diverse projects which leaded me to improve my knowledge and understanding of Seismology.

I would also like to thank Assoc. Prof. Dr. Ali Özgün Konca for his continuous help and feedback throughout the study.

I am grateful to Dr. Eric Bergman for sharing his multiple event relocation code "mloc" and Ezgi Karasözen for the assistance whenever I needed.

My special thanks are extended to Dr. Caner Koca for his support and Dr. Rengin Gök for her encouragement and useful critiques during this study.

My sincere thanks also goes to Zeynep Yılmaz, Nilay Başarır and Doğan Baştürk for all their support and company. I also wish to acknowledge the help provided by Dr. Uğur Mustafa Teoman and Dr. Metin Kahraman.

Finally, I must express my very profound gratitude to my family and to my partner for providing me with unfailing support and continuous encouragement throughout my years of study and through the process of researching and writing this thesis. This accomplishment would not have been possible without them. Thank you.

ABSTRACT

RELOCATION OF EARTHQUAKES IN THE SALT LAKE REGION USING THE HYPOCENTROIDAL DECOMPOSITION (HDC) METHOD

Central Anatolia is a relatively stable region unlike the other regions under the influence of major tectonic regimes in Turkey. For that reason, the number of seismic instruments installed by regional earthquake monitoring centers are insufficient on determining and locating earthquakes accurately that are below a certain magnitude in that region. In this study this issue is overcome by building a merged catalog from the data of Kandilli Observatory and Earthquake Research Institute's (KOERI) permanent broadband seismic network, temporary broadband seismic network deployment as a part of the "Continental Dynamics: Central Anatolia Tectonics (CD-CAT)" project, which was installed in the South and Central Anatolian Region along with the data obtained from International Seismological Centre (ISC). The multiple event relocation technique "mloc" which is based on hypocentroidal decomposition (HDC) algorithm is applied by utilizing the phase arrival time catalog that was specifically crafted for the study area. Thus, seismic activity surrounding the Salt Lake Fault Zone (SLFZ) and Ecemiş Fault Zone (EFZ) in between 1th of June 2013 to 15th of May 2015 are relocated and calibrated. 1-D crustal velocity models are developed for the interest regions, thereby hypocentral parameters as well as the corresponding uncertainties of the total number of 394 earthquakes are extensively evaluated and classified in order to unravel the tectonic features and seismicity of the Salt Lake Region.

ÖZET

TUZ GÖLÜ BÖLGESİ DEPREMLERİNİN ODAKSAL AYRIŞTIRMA (HDC) YÖNTEMİYLE YENİDEN KONUMLANDIRILMASI

İç Anadolu Bölgesi, Türkiye'nin önemli sismik rejimlerinin etkisi altında bulunan diğer bölgelere nispeten daha durağan bir bölgedir. Bu nedenle, bölgesel deprem izleme merkezleri tarafından kurulan sismik istasyonların sayısı, belirli bir büyüklüğün altında gerçekleşen depremlerin tespitinde ve konumlarının doğru olarak belirlenmesinde yetersiz kalmaktadır. Bu sorun; Uluslararası Sismoloji Merkezi (ISC) kataloğunun, Kandilli Rasathanesi ve Deprem Araştırma Enstitüsü kalıcı genişbant sismik ağının ve geçici genişbant CD-CAT sismik ağının Güney ve Orta Anadolu Bölgesine sağlamış olduğu verilerin birleştirilmesiyle oluşturulmuş bir katalog ile aşılmıştır. Çalışma alanı için özel olarak hazırlanmış olan faz varış zamanı kataloğundan yararlanılarak odaksal ayrıştırma (HDC) algoritmasını temel alan bir çoklu aktivite yeniden konumlandırma tekniği olan "mloc" uygulanmıştır. Böylece, 1 Haziran 2013 - 15 Mayıs 2015 tarihleri arasında Tuz Gölü Fay Zonu (TGFZ) ve Ecemiş Fay Zonu (EFZ) bölgelerini çevreleyen deprem aktivitesi yeniden konumlandırılmış ve kalibre edilmiştir. Tuz Gölü Bölgesi'nin tektonik yapısı ve depremselliğini aydınlatmak amacıyla, ilgilenilen bölgelerin 1 boyutlu kabuk hız modelleri geliştirilmiş, dolayısıyla toplam 394 deprem, odak parametreleri ve bu parametrelere karşılık gelen belirsizlikleri ile birlikte kapsamlı bir şekilde değerlendirilmiş ve sınıflandırılmıştır.

TABLE OF CONTENTS

ACKNOWLEDGEMENTS . . . iii
ABSTRACT . . . iv
ÖZET . . . v
LIST OF FIGURES . . . viii
LIST OF TABLES . . . x
LIST OF SYMBOLS . . . xi
LIST OF ACRONYMS/ABBREVIATIONS . . . xii
1. INTRODUCTION . . . 1
2. TECTONIC SETTING of the CENTRAL ANATOLIA . . . 2
3. HDC METHOD FOR CALIBRATED LOCATIONS . . . 10
3.1. Direct Calibration . . . 13
3.2. Indirect Calibration . . . 14
3.3. Data Usage . . . 14
3.4. Outlier Removal . . . 15
3.5. Depth Determination . . . 17
3.6. Earthquake Location Accuracy Codes . . . 17
3.6.1. Ground Truth: The G Class . . . 18
3.6.2. Calibrated Events: The C Class . . . 18
3.6.3. Network Geometry Criteria: The N Class . . . 19
3.6.4. Uncalibrated Events: The U Class . . . 20
3.6.5. Scale Length and Confidence Levels . . . 20
4. APPLICATION . . . 21
4.1. Data Compilation . . . 21
4.2. Refining Bulletins . . . 24
4.3. Determining Cluster Boundaries . . . 24
4.4. 1-D Velocity Model Assessment . . . 25
4.5. Relocating Clusters . . . 25
4.6. Determining Depths . . . 28
5. RESULTS . . . 29

5.1. Analysis of Sub-region A 31
5.2. Analysis of Sub-region B 43
6. DISCUSSION 56
7. CONCLUSIONS 60
REFERENCES 62

LIST OF FIGURES

Figure 2.1. Major tectonic structures in Turkey 2

Figure 2.2. GPS velocity vectors for Anatolian Plate 3

Figure 2.3. Simplified geological map of CACC 5

Figure 2.4. Evolution of CACC during the late-Cretaceous 6

Figure 2.5. Poly-genetic volcanoes located in Central Anatolia 7

Figure 2.6. Illustration showing developement along EFZ 9

Figure 3.1. Geometry of the HDC approach 12

Figure 3.2. Schematic outline of direct calibration 13

Figure 3.3. Schematic outline of indirect calibration 14

Figure 3.4. Empirical reading error 15

Figure 3.5. GCNU accuracy classification system 18

Figure 4.1. Stations used in the study 22

Figure 4.2. Events used in the study 23

Figure 4.3. The workflow followed in the study 27

Figure 5.1. Overview of the relocation results 30

Figure 5.2. Travel time curves of Sub-region A 31

Figure 5.3. Ray paths used to locate hypocentroid of the Sub-region A 32

Figure 5.4. Map of empirical path anomaly over spread (P_g, Sub-region A) . . 34

Figure 5.5. Map of empirical path anomaly over spread (S_g, Sub-region A) . . 35

Figure 5.6. Epicenters and depths of earthquakes relocated in Sub-region A . 37

Figure 5.7. Travel time curves of Sub-region B 43

Figure 5.8. Ray paths used to locate hypocentroid of the Sub-region B 44

Figure 5.9. Map of empirical path anomaly over spread (P_g, Sub-region B) . . 46

Figure 5.10. Map of empirical path anomaly over spread (S_g, Sub-region B) . . 47

Figure 5.11. Epicenters and depths of earthquakes relocated in Sub-region B . 49

Figure 6.1. The map illustrating notable findings in the study. 57

Figure 6.2. The map comparing the findings on velocity structure 58

LIST OF TABLES

Table 3.1. The C class accuracy codes 19

Table 5.1. Amount of relocated and calibrated events 29

Table 5.2. Crustal velocity model used in Sub-region A 31

Table 5.3. Statistics of the relocation results for the Sub-region A 38

Table 5.4. Crustal velocity model used in Sub-region B 43

Table 5.5. Statistics of the relocation results for the Sub-region B 50

LIST OF SYMBOLS

dts_i	Travel time residual of a certain station phase
$\overline{dts}$	Empirical path anomaly
eci	Empirical reading error
eci_i	Empirical reading error of a certain station phase
S_n	Robust estimate of spread
XX	Scale length
σ	Standard deviation

LIST OF ACRONYMS/ABBREVIATIONS

1D	One Dimensional
AES	Aegean extensional system
AFAD	Republic of Turkey Prime Ministry Disaster and Emergency Management Authority
CACC	Central Anatolian Crystalline Complex
CAFS	Central Anatolian Fault System
CVP	Cappadocian Volcanic Province
CD-CAT	Continental Dynamics: Central Anatolia Tectonics Project
DD	Double Difference
DDA	Network Code of Disaster and Emergency Management Presidency
EAFS	East Anatolian Fault System
EFZ	Ecemiş Fault Zone
HDC	Hypocentroidal Decomposition
ISC	International Seismological Centre
ISK	Network Code of Kandilli Observatory and Earthquake Research Institute
İAESZ	İzmir-Ankara-Erzincan Suture Zone
İEFS	İnönü-Eskişehir Fault System
JHD	Joint Hypocenter Determination
KOERI	Kandilli Observatory and Earthquake Research Institute
mloc	Multiple Event Relocation Program
NAFS	North Anatolian Fault System
NVC	Niğde Volcanic Complex
P	P wave
RETMC	Regional Earthquake-Tsunami Monitoring Center
SLFZ	Salt Lake Fault Zone
S	S wave
YB	CD-CAT Network Code

1. INTRODUCTION

Central Anatolian Plateau carries out its westward tectonic motion along with the Anatolian plate without significant inner deformation or major faulting [1–3]. However, Central Anatolian Crystalline Complex (CACC) which is bounded by the Salt Lake Fault Zone (SLFZ) to the west and Ecemiş Fault Zone (EFZ) to the south are seismically very active and have been producing relatively small earthquakes (M<5) throughout the Salt Lake Region. Monitoring and recording these seismic activity, particularly the earthquakes smaller than magnitude 2 requires a good network coverage and proximity. However, due to comparatively stable nature of the Central Anatolia in contrast with the regions under the influence of major tectonic regimes in Turkey, the dedicated number of instruments installed by "Regional Earthquake and Tsunami Monitoring Center" (RETMC) and "Republic of Turkey Prime Ministry Disaster and Emergency Management Authority" (AFAD) in order to monitor the Salt Lake and its surroundings is not adequate to detect and locate the earthquakes that is referred above.

Main purpose of this study is to relocate and then calibrate the hypocenter locations of the earthquakes occurred in the interest region using the mloc program [4, 5] which is based on hypocentroidal decomposition (HDC) algorithm [6], by taking advantage of the abundance of data combined from the International Seismological Centre (ISC) and the temporary CD-CAT network which is a very dense local seismic network deployed in southern Turkey and monitored the region in between 1th of June 2013 to 15th of May 2015. In comparison to other multiple event relocation methods, the mloc technique has the advantage of minimizing the location bias and quantifying the uncertainty in each relocation solution as a part of the calibration process. In that way, reassessed and calibrated catalog of earthquake hypocenter locations crafted for the study area will contribute significantly to the future relocation studies regarding the Salt Lake Region by providing reference events that are extensively evaluated and then quantified with a classification system.

2. TECTONIC SETTING of the CENTRAL ANATOLIA

Anatolia is a composite structure consisting multiple tectonic regimes under the influence of Arabian and African plates and Hellenic and Cyprian arcs [7] (Figure 2.1). To the east, plate boundaries between Arabian and Anatolian plates converge with a possibility of small extension in the absence of normal faulting where mainly left-lateral strike-slip motion is observed [8]. The major tectonic boundaries of the Anatolian Plate; North Anatolian Fault System (NAFS) and East Anatolian Fault System (EAFS) are deemed as a result of the collision of Anatolian and Arabian tectonic plates during the late Miocene [9, 10]. Extensional pullback movements from the Hellenic-Cyprus trench system with the increasing rate of motion towards the Hellenic Arc [8] are accompanied by counterclockwise rotational-wrench tectonics [3, 11–13] and lead to slab-rollback movement of the Anatolian Plate toward west (Figure 2.2). In addition, the compression from northward motion of the Arabian Plate toward Eurasia [1, 14] also contributes to westward motion of the Anatolian plate with the help of NAF and the EAF systems colliding near Bingöl-Karlıova triple junction.

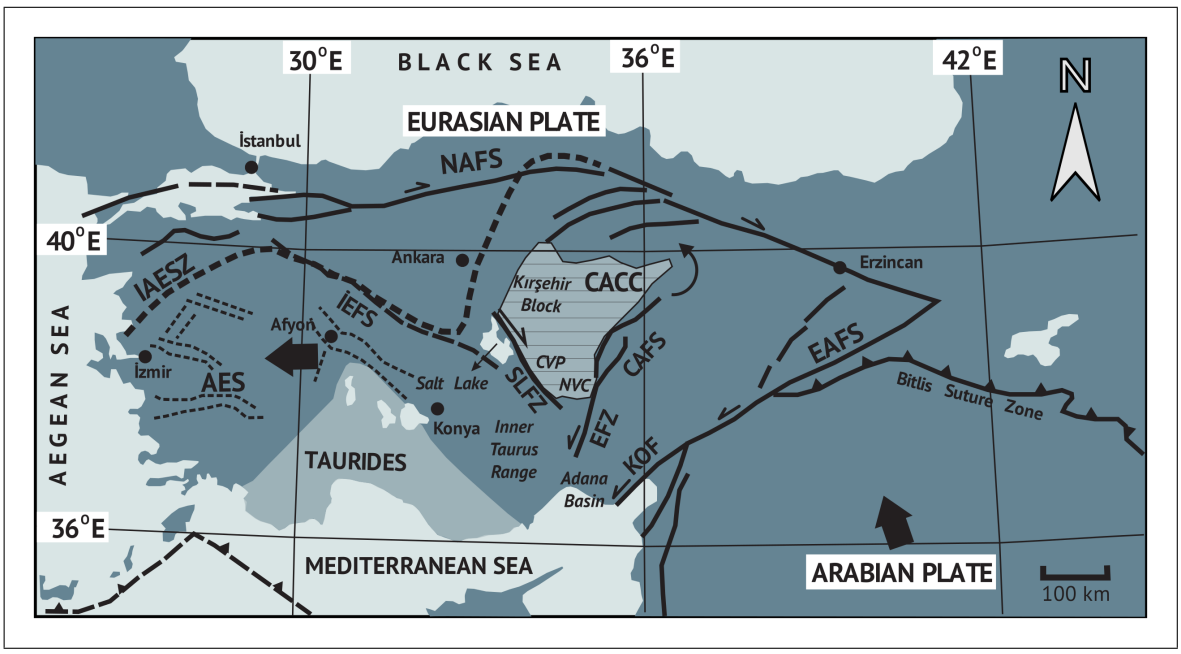

Figure 2.1. Map showing the major tectonic structures in Turkey [15] and modified after [16].

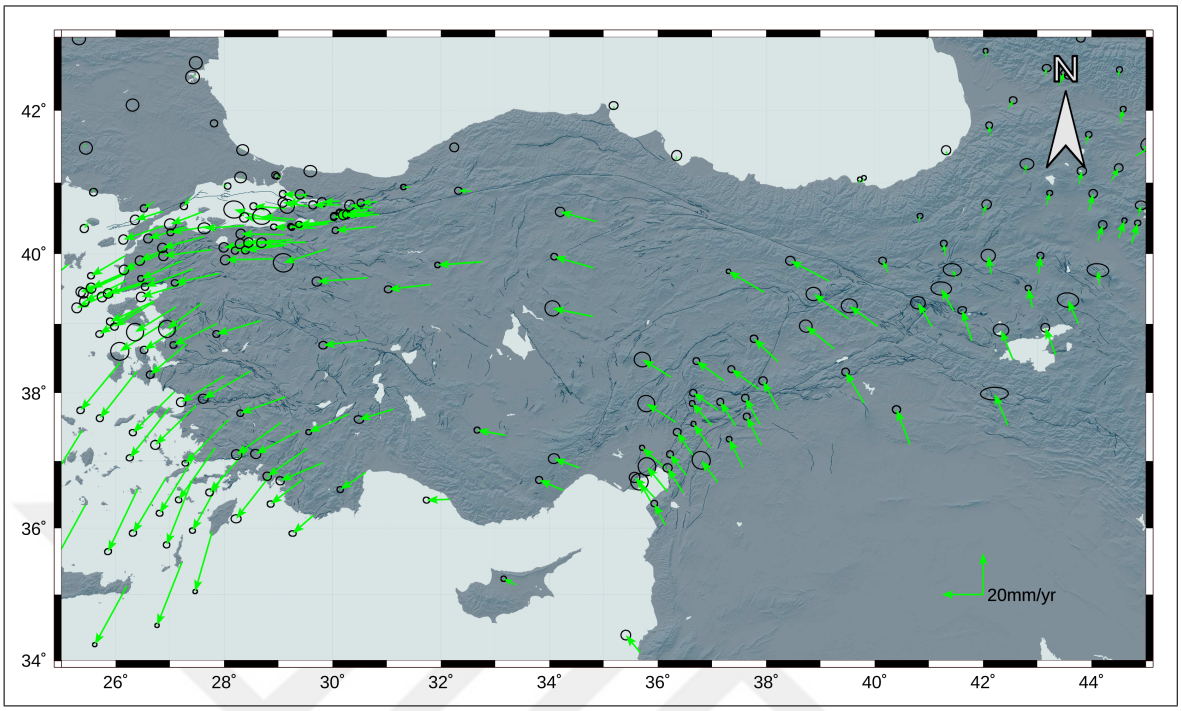

Figure 2.2. Map showing GPS velocity vectors for Anatolian Plate with %95 percent confidence ellipses [8]. Active faults modified from [17].

Tectonic behavior and the Moho depth of the Anatolian Plate varies from east to west; observed as thicker compressional regime in the east ($\leqslant$50 km), stable in the central Anatolia ($\sim$37 km average) and extensional tectonics with a thinner crust in west ($\leqslant$ 30 km) revealing a transition to the Aegean Extensional System [7, 15, 18].

The Central and Eastern Anatolian plateaus together are the world's third largest orogenic plateau. Uplift mechanisms observed in this regions are associated with the oceanic slab-break off and tearing during middle to late Miocene, through the Cyprian arcs with the influence of the African plate [18]. The Central Anatolian region which is part of the Anatolian block contains tectonic attributes including the Inner Taurus range, the Adana basin, Salt Lake Fault Zone (SLFZ), Ecemiş Fault Zone (EFZ) and Central Anatolian Fault System (CAFS) as part of the Cappadocian Volcanic Province (CVP) [19] and Kırşehir Block as well as Niğde Volcanic Complex (NVC) which are also enclosed by Central Anatolia Crystalline Complex (CACC) (Figure 2.1 and 2.3).

Regional structure of the CACC (Figure 2.3) consists of crystalline rocks; Mesozoic - Paleogene sedimentary, ophiolites, magmatic intrusions or metamorphic rocks subjected to deformation since Eocene - early-Oligocene (Ma 30) by folds, thrusts and trans-current faults [20, 21]. Evolution of the CACC is linked with the Tavşanlı high pressure zone situated at ∼100 kilometers west where a paired metamorphic belt is formed with an active intraocenaic thrusting/subduction [22] during the late-Cretaceous (Figure 2.4). In addition, northern boundary of the CACC converged and collided into the Pontides, which resulted in three separated blocks; Niğde Massif (containing CVP and NVC), Akdağ Massif and Kırşehir Massif, which are assumed to represent the nowadays structure [21, 23].

The CVP is considered as a well preserved volcanic landscape displaying the transition from collision to post-collision volcanism. Bimodal type of volcanism observed in NVC and CVP is associated with the extensional tectonics. Bimodal volcanism which took important part during magma genesis is proposed to develop in a post-collisional activity that is caused by ascending asthenosphere [19].

The dextral Salt Lake and sinistral Ecemiş faults which resulted from the north-south compression [21, 23], are the most noteworthy sources of seismic activity in the region, even though there is no observation of earthquakes above magnitude 5 since the start of the instrumented era of seismology. The Salt Lake Fault bounds the north-eastern part of the Salt Lake basin with a 200 kilometers long NW trending fault line [24–26], towards NE trending 100 kilometers long Ecemiş Fault without an intersection [27, 28]. Poly-genetic volcanoes scattered to the west of the Salt Lake Fault, volcanic centers located in the eastern part of CVP and along the Ecemiş Fault indicates the regional scale of the deformation [29] (Figure 2.5).

The CAFS is a 700 kilometers long, 2 to 80 kilometers wide sinistral fault system. It is a very young neotectonic structure and assumed to originate from the reactivation and propagation of the older paleotectonic formation named Ecemiş Corridor [28].

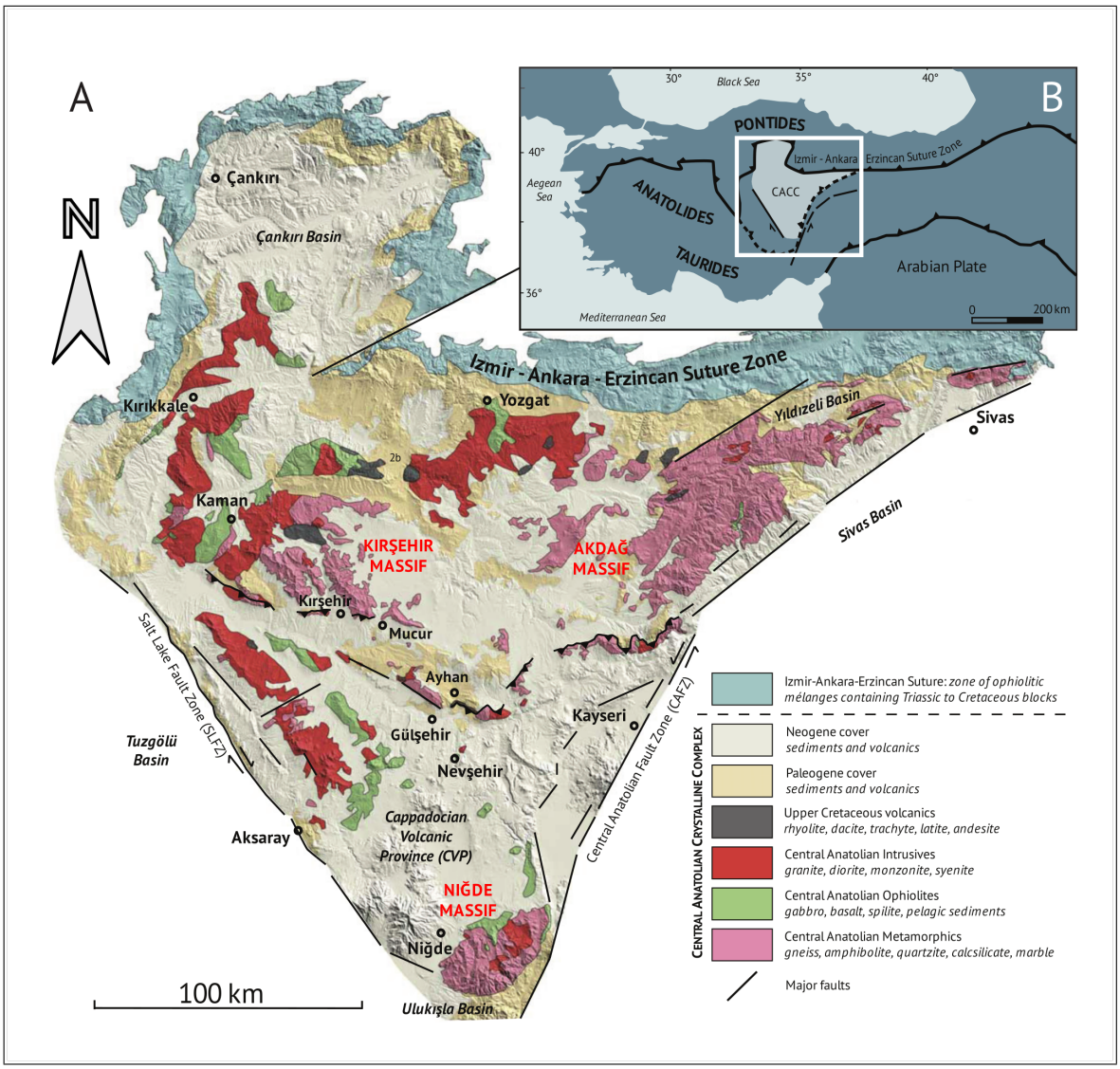

Figure 2.3. A: Simplified geological map of the CACC, B: Simplified tectonic outline of Turkey, modified from [21].

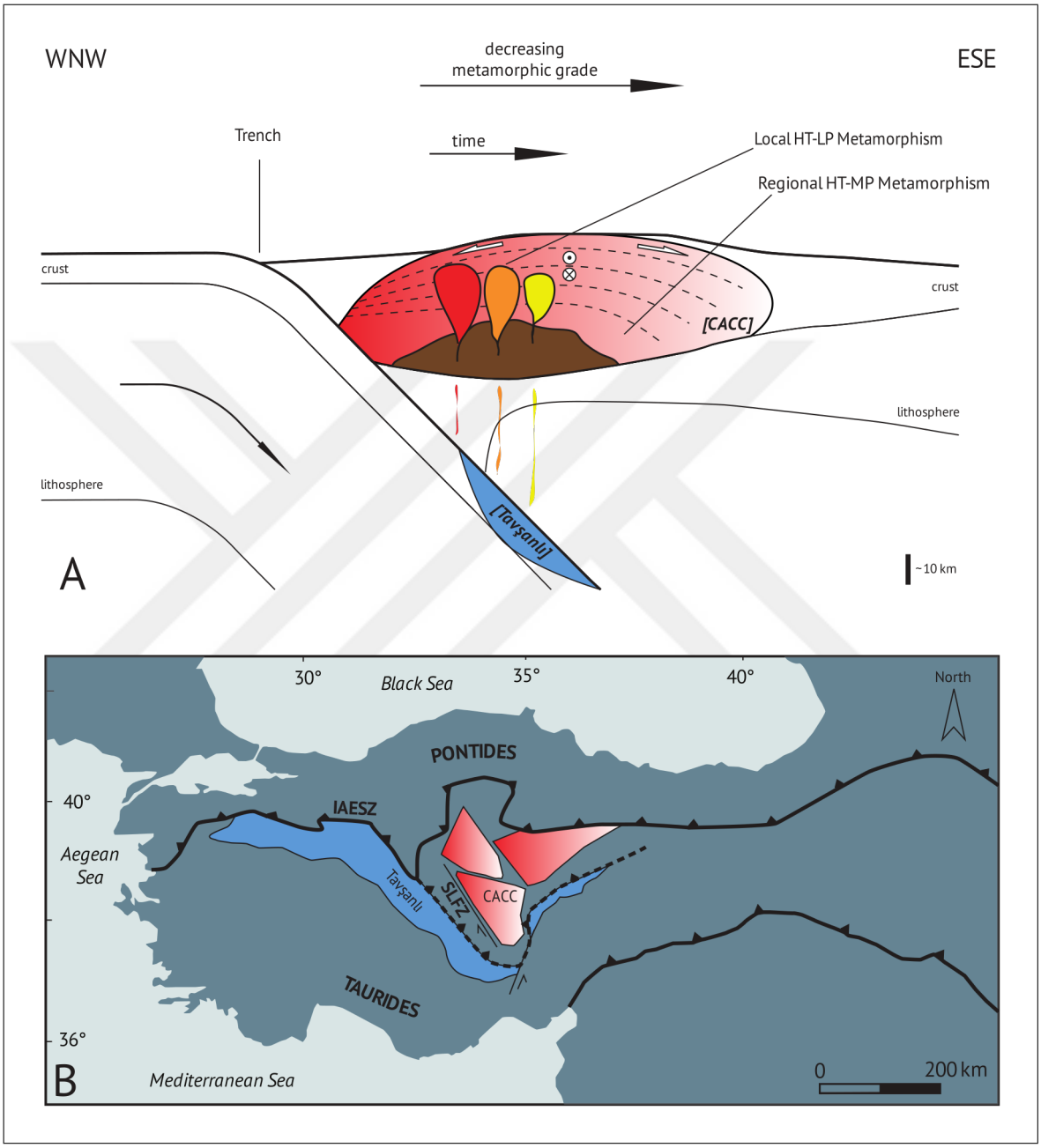

Figure 2.4. A: Illustration of E-W lithospheric section showing local high-temperature-low-pressure (HT-LP) and regional high-temperature-moderate-pressure (HT-MP) metamorphic grading, B: Simplified map of Turkey showing the paired metamorphic belt of the CACC and its evolution during the late-Cretaceous [21].

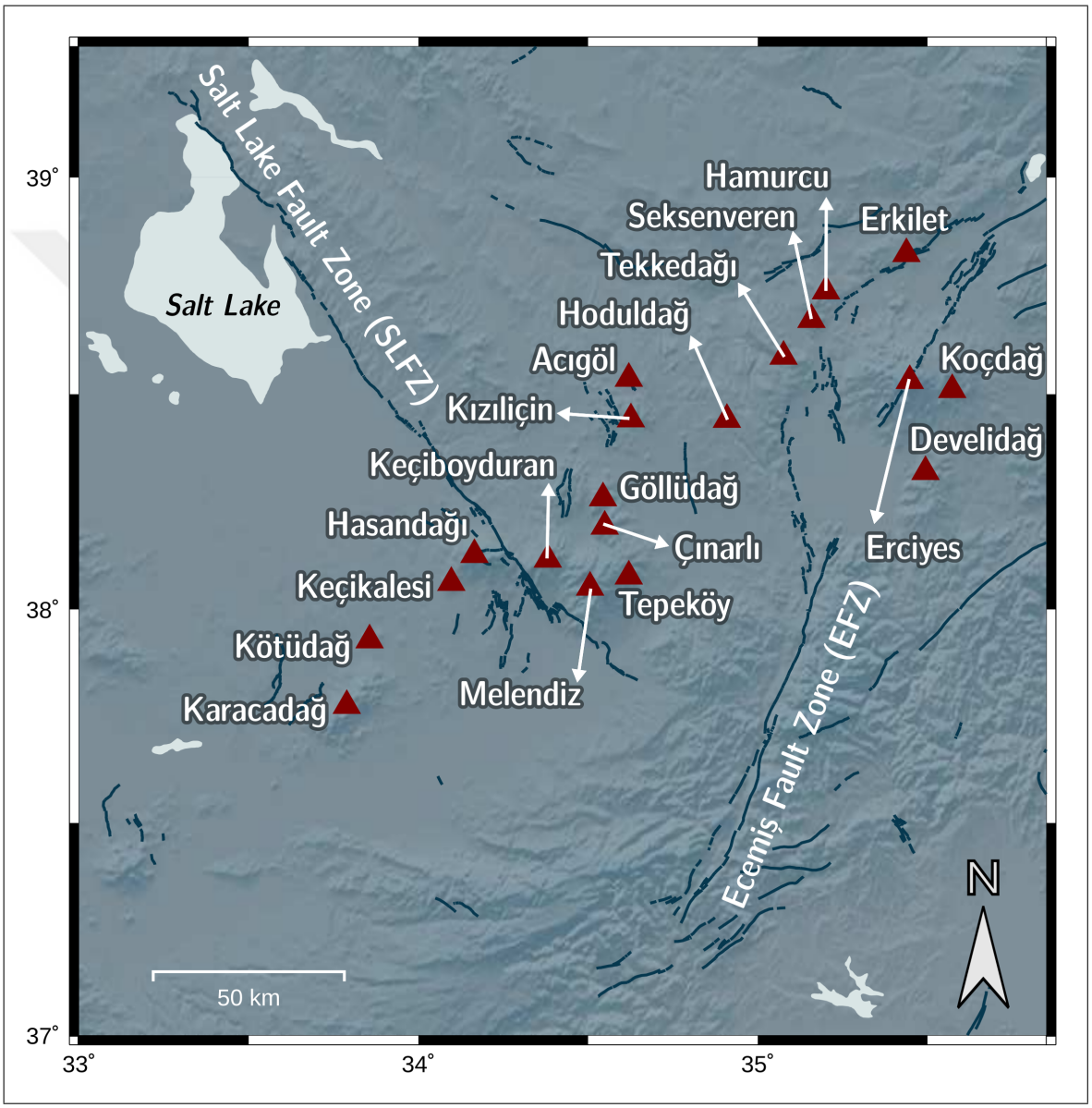

Figure 2.5. Poly-genetic volcanoes located in the Central Anatolia. Volcanoes are denoted with dark red triangles, modified from [29].

Niğde Massif is proposed to go through two complete cycles of burial and exhumation of its metamorphic basement and sedimentary rocks during orogenesis from Late Cretaceous to Miocene. This phenomenon, which is observed in the Niğde Massif and Ecemiş fault system is a good example of yo-yo tectonics. Here, the vertical motion of a yo-yo is used as an exemplification to illustrate the upward and downward vertical motion occurred during the burial and exhumation. Aforementioned type of structural behaviour is proposed to be impelled by transpressional and transtensional intercontinental strike-slip deformations [30].

Development process of the Ecemiş Fault Zone and Niğde Massif is shown in Figure 2.6. First phase of development includes transpressional deformation of Mesozoic sedimentary rocks by burial and heating during Late Cretaceous (91-60 Ma) which resulted in high-grade metamorphic basement; then followed by the transtensional deformation and erosion which led unroofing of early Tertiary deposition including massif-derived clastic material from the marine basin situated along the CAFS (Figure 2.6.A). The beginning of the second cycle of yo-yo tectonics took place between late Eocene through early Miocene times (50-20 Ma) by the reburial of basement as well as transpressional folding, shearing and metamorphism of the cover sedimentary rocks along early Ecemiş fault [30] (Figure 2.6.B). The last exhumation occurred in the Niğde Massif and the lower Tertiary sedimentary rocks during transtension along Ecemiş fault in the middle Miocene (17-9 Ma) and finalized the cycles of burial and exhumation. The Ecemiş fault increased its length and offset in this period (Figure 2.6.C). The prior left-lateral strike-slip transtensional faulting observed in the Miocene was succeeded by a transtensional/extensional transformation on the Ecemiş Fault, displaying the part of the tectonic escape of Anatolian Block in the past 5 million years. [30, 31] (Figure 2.6.D).

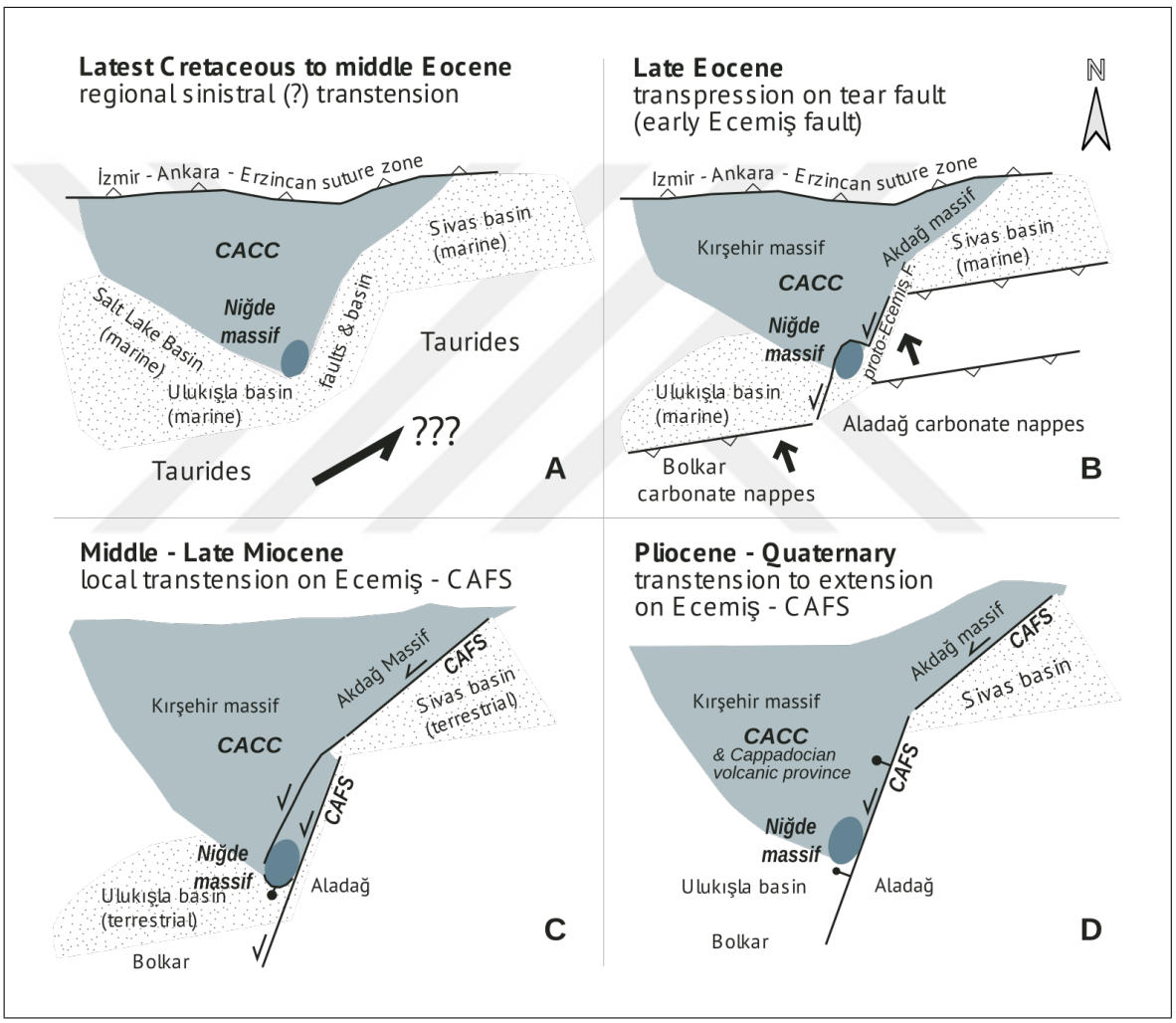

Figure 2.6. Illustration showing the tectonic developement along the EFZ and Niğde Massif [30] and modified after [31].

3. HDC METHOD FOR CALIBRATED LOCATIONS

Determining accurate locations of seismic activity is crucial as they carry out information regarding the geology and the tectonic features of the surrounding region. Earthquake location problem consists of finding a suitable earth model for the study region, having a well positioned seismic network covering the activity which provides the arrival time data, and, the data itself as reliability of the information directly affects the accuracy of the result.

There are different approaches to resolve the earthquake location problem and their distinction revolve around putting an emphasis on the earth model and the way they deal with the arrival time data sets. Most of the non-linear solutions for the single or multiple event location approaches based on the Geiger's Method [32] which aims to linearize the slight changes in the source coordinates to the travel time residuals. Seismic events can be located independently or jointly by using some form of Geiger's Method. The joint hypocenter determination method (JHD) [33–35] determines the station corrections from the difference between observed and calculated travel times of every single event by using the entire data set, then calculate the origin times and hypocenteral parameters of multiple of events by adding those station residuals. On the other hand, the double difference (DD) method [36] uses the difference of observed and calculated travel times of event pairs at a common station instead. Therefore, the double difference alghoritm minimizes the path related errors without a need to use station corrections. In contrast to JHD and DD, the multiple event relocation technique Bayesloc [37] takes a different path on solving the non-linear location problem by employing the Bayesian hierarchical statistical modeling. Algorithm of the Bayesloc decomposes the location problem into a travel time model, an arrival time model and a prior model for all parameters, in order to employ forward calculations that will be used for the estimation of: joint probability of event locations, corrections to travel time predictions and precision of arrival time assessments by utilizing "Markov-Chain Monte Carlo" method.

For the cases of seismic clusters, such as mainshock-aftershock sequences, earthquakes that occured on the same fault segment in different time-line or engineered explosions, a multiple event relocation approach can be useful. The main reasoning behind all multiple event relocation methods is the way they take advantage of the similarity of raypaths, originated from closeby earthquakes for a common station [4]. Thus, it is an approach to reduce velocity model related errors.

In this study, multiple event relocation program mloc (Bergman and Solomon, 1990; Walker et al., 2011) [4,5] which is based on hypocentroidal decomposition (HDC) algorithm introduced by Jordan and Sverdrup [6] (1981) is used to relocate and calibrate earthquake clusters. The term "calibrated" used to define emphasis on bias-free solutions, therefore, minimizing uncertainties of locations and making them realistic in statistical sense [38].

HDC algorithm operates iteratively and it breaks down the problem into two inversions in order to initiate relocation process:

(i) The first inversion is for computing the cluster vectors, which represent the relative location of each event to the current position of the hypocentroid (Figure 3.1). The vectors are defined in kilometers and seconds and entirely derived from arrival time differences of the same seismic phase readings of cluster events. As a result, travel time errors are not carried out with the cluster vectors.

(ii) The second inversion is for the hypocentroid, which is defined as the geometrical average of the cluster events (Figure 3.1). Hypocentroid is defined in geographic coordinates and Coordinated Universal Time (UTC). Hypocentroid location is improved after each iteration by using the all data from cluster events, therefore, it is more susceptible to unknown bias originated from the theoretical travel times.

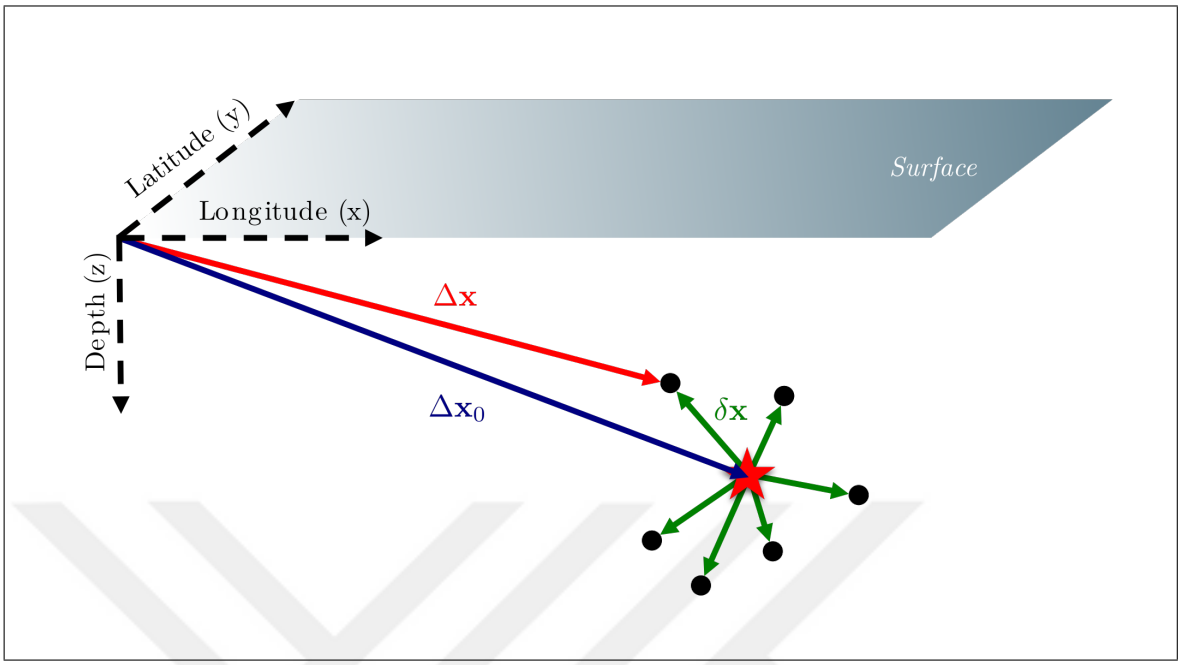

Figure 3.1. Geometry of the HDC approach. 0 point is the initial solution of a certain event, black circles represent each event in the cluster and the red star is the hypocentroid. Displacement vector of a certain event (Δx) is sum of the displacement vector of the event (Δx_0) and the cluster vector (δx) [39].

In short, the first iteration computes cluster vectors and then they are acted on the hypocentroid (derived by taking the geometrical average of the initial single-event locations on the first run) in order to obtain absolute coordinates for each event. Then the second iteration takes part where improved hypocentroid is calculated in relation to adjusted event locations. These two inversions completes an iteration cycle and cycle lasts until it reaches to the convergence.

Up to here, geographic location solutions are contaminated with the bias from calculation of hypocentroid as it heavily relies on the travel time model. Removing or reducing the bias is possible by applying a form of calibration technique to the cluster. There are two different techniques to calibrate a cluster: direct and indirect calibration, and they will be investigated in the following sections 3.1 and 3.2.

3.1. Direct Calibration

Direct calibration technique depends on abundance of the near-distance data and good coverage of recording stations surrounding the hypocentroid. Specifically, crustal phases P_g and S_g originated from less than 2° distance are used for determination of the hypocentroid. Using near distance arrival time data helps on reducing ray-path lengths, hence the travel time error from the unknown velocity structure. Therefore, we end up having minimized bias on the hypocentroid that is leading better relocation solutions (Figure 3.2).

Having a well situated network for direct calibration is also useful for constraints on depth, as, direct P_g and S_g waves from a very near source can yield accurate estimations.

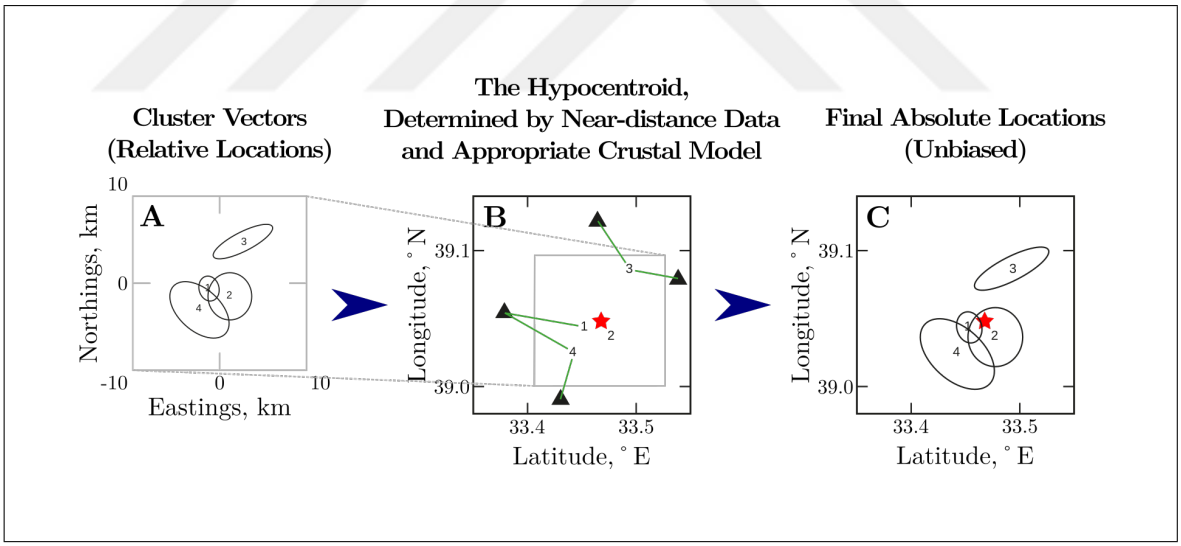

Figure 3.2. Schematic outline of direct calibration [38].

3.2. Indirect Calibration

Indirect calibration technique comes into play when ground-truth data or equivalent are available. In these cases, we can use reference events with well-known location and origin time (e.g. ground truth events, man-made explosions, calibrated events) by shifting the cluster in space and time (Figure 3.3). Shifting is done by applying the mislocation vector which is determined by the calibration events.

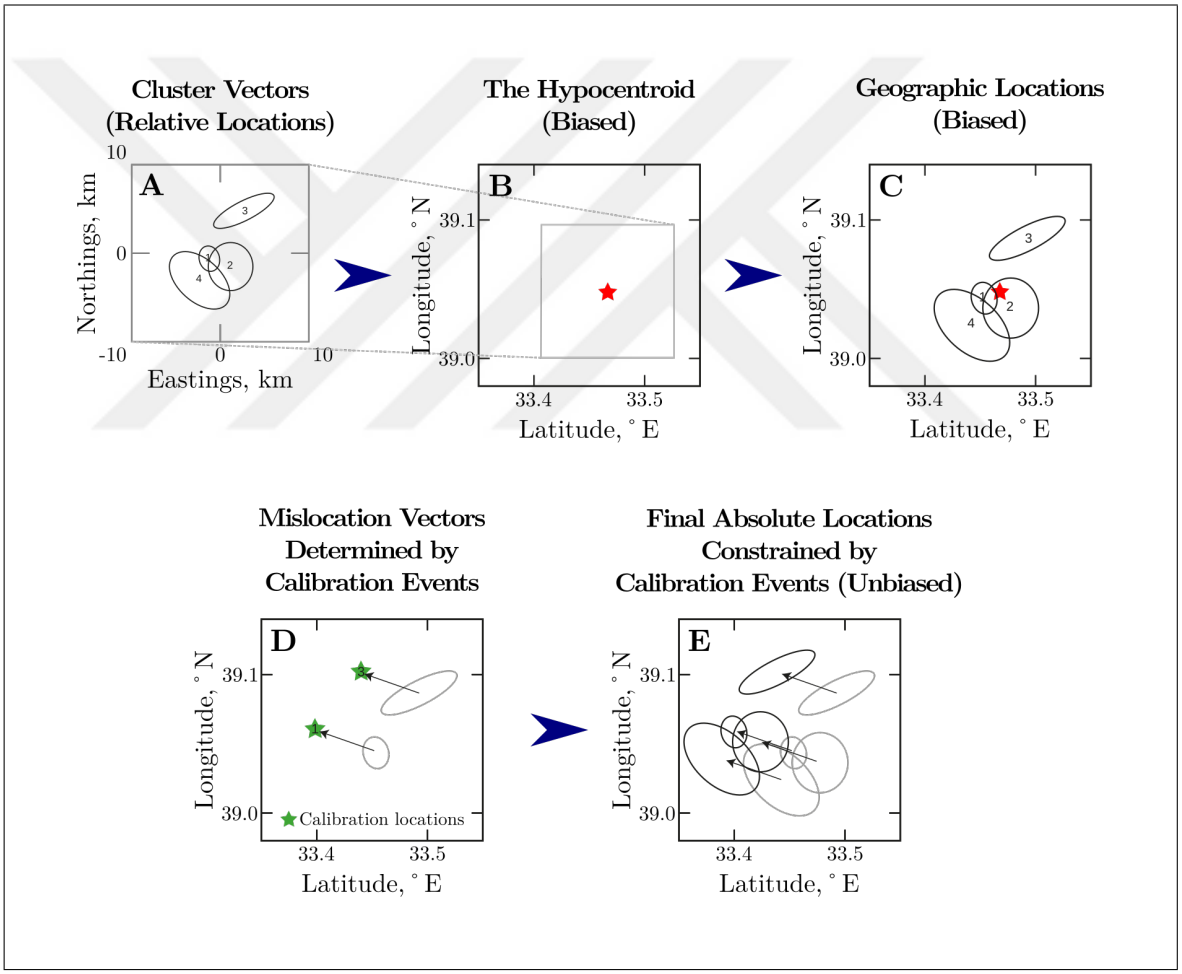

Figure 3.3. Schematic outline of indirect calibration [38].

3.3. Data Usage

The program mloc uses standard seismic bulletin arrival times to relocate events. One of the advantage of the mloc is its ability to process customized clusters. A cluster can be formed by combining mainshock-aftershock sequences, older seismic

activity, data recorded from temporary seismic networks, ground truth events and/or man-made explosions for a specified region. The mloc algorithm is well-suited for relocating up to 200 events within a geographic extent of 100 kilometers or less. Main reason for such limitation is to keep the connectivity of the cluster at an ideal level, as repeated observations are an important aspect of the algorithm. In addition to that, it is expected to have near-source readings for direct calibration technique.

3.4. Outlier Removal

Traditionally, earthquake location algorithms focus on the residuals calculated against a reference travel time model when identifying outliers. Unlike others, the multiple event relocation program mloc put importance on consistency of repeated readings. When working on clusters, it is common to observe same type of seismic phases from multiple of events for a common station. This empirical phenomenon allows us to implement a statistical analysis, which is referred in this context as "Empirical reading error" [38] that assists program and analyst to distinguish useful data from the bad by estimating the spread of residuals in relation with the mean of residuals and weight the arrival time data (Figure 3.4).

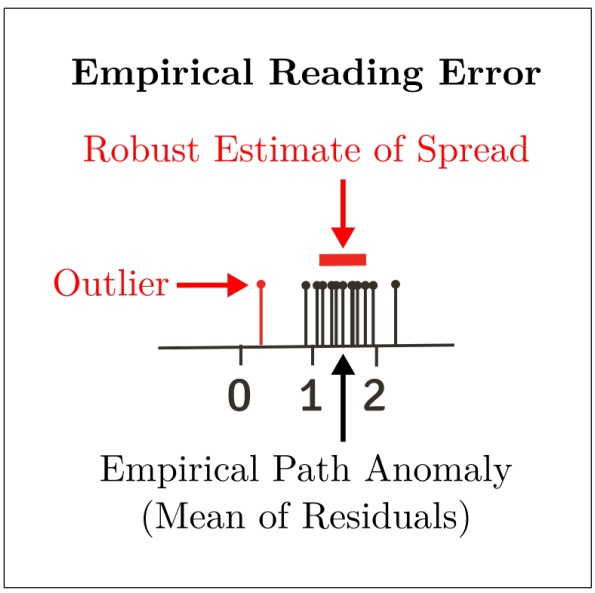

Figure 3.4. Empirical reading error [38].

Spread is determined by using the robust estimator S_n proposed by Croux and Peter in 1992 [40] and defined as:

$$S_n = c_n \, 1.1926 \underset{(i=1,\ldots,n)}{lomed} \underset{(j\neq 1)}{lomed} |x_i - x_j| \tag{3.1}$$

where c_n is a correction term used in small sample sizes, the factor 1.1926 establishes consistency at normal distribution and "lomed" is the low median.

Empirical reading error of a station phase "i" or "eci_i" (i.e. P_g phase arrival time of an event on ANTO station) is calculated with the following equation:

$$eci_i = \frac{dts_i - \overline{dts}}{S_n} \tag{3.2}$$

where dts_i is the travel time residual of the station phase "i" which obtained by taking the difference between observed and theoretical arrival times. $\overline{dts}$ represents the empirical path anomaly, in other words, the mean of residuals of the same phase type as "i" for the common station (i.e. mean of residuals of every P_g phase observed on ANTO station). The S_n should not be confused with the type of earthquake phase. In this context it is the estimate of spread of the arrival-time residuals for the same station phases. The spread (S_n) is determined by using the Equation 3.1.

Eliminating the outliers are done gradually. Data with the highest empirical reading error (eci) are removed first, then after a relocation, the distribution of the eci is checked back. Main reason for removing outliers incrementally is to prevent rejection of the good data. As a result of these iterations, it is expected to have a distribution approached to a Gaussian distribution that is demeaned and normalized.

These steps of cleaning outliers remain until all residuals are within 3σ of the mean where the empirical reading error (eci) is used as the estimate of σ [38].

3.5. Depth Determination

The HDC method fall short on treating the focal depth as a free parameter in the relocation process. This issue might arise from the lack of completeness of the near-distance readings or teleseismic depth phases (e.g. pP, sP, SS) that is necessary for the inversion determining cluster vectors regarding the focal depth [38]. Thus, best approach to overcome incompleteness of depth related data would be fixing it for the whole cluster in the relocation process and then developing a routine for determining focal depth of each event separately. As suggested in the Section 3.1, using direct P_g and S_g arrivals from very near source can be useful for evaluating focal depth of each event in the cluster.

3.6. Earthquake Location Accuracy Codes

The mloc program is specifically tailored for calibrated relocation studies, since, it prioritizes providing hypocentral parameters with realistic estimates of uncertainites that is minimally biased. Relocation solutions are provided with an extended classification system based on (Bondar et al., 2004) [41], also known as GTX formulation. In addition to the GTX formulation, mloc uses the GCNU classification system includes information of the accuracy of hypocentral parameters, focal depth and origin time, rather than only the epicenter. The name "GCNU" comes from the first letters of each accuracy class (Figure 3.5) which will be examined in the following subsections. The general form in this system contains four characters; first one indicates accuracy class and second one states which parameters can be considered calibrated. Third and fourth characters are numerical and they represents accuracy of the epicenters in kilometers.

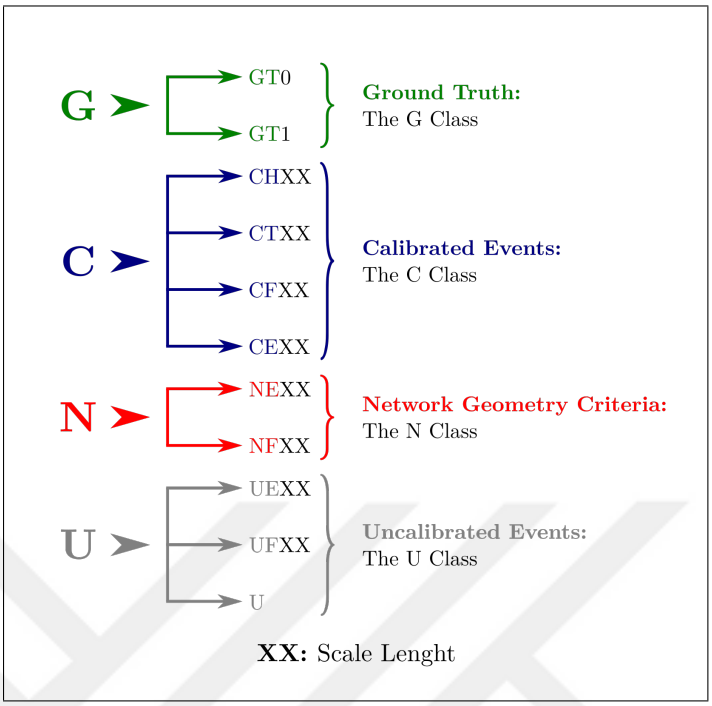

Figure 3.5. Diagram showing classes and accuracy codes of the GCNU accuracy classification system

3.6.1. Ground Truth: The G Class

The G class can be used as either GT0 or GT1 form. Ground truth events which are known very well with all four hypocentral parameters are considered as GT0. These type of events have very low uncertainties that is almost negligible.

In some cases, ground truth events may not satisfy the necessary criteria regarding uncertainties for GT0. Thereby, ground truth events with scale length 1 can be defined in GT1 category since events with higher uncertainties are not considered as ground truth.

3.6.2. Calibrated Events: The C Class

Location calibration takes major part of the mloc algorithm where determining random error and uncertainties in hypocentral parameters are the main concern.

For this reason, accuracy codes defined for the calibrated events put importance on understanding which parameters can be considered bias free.

There are 4 different cases for defining the accuracy codes for the class C which also can be seen from the Table 3.1:

- CH: "H" stands for hypocenter and all hypocentral parameters are calibrated.
- CT: "T" refers travel time. Depth is fixed, epicenter is calibrated and origin time is estimated by using local-distance data relative to an uncalibrated depth for this classification.
- CF: "F" represents focal depth. Epicenter and focal depth are calibrated. This classification is possible when we estimate the location and the depth with an additional method (i.e. location constrained with an InSAR study and depth evaluated through a waveform analysis) and there are no near-source stations to determine origin time.
- CE: "E" is for epicenter. Only the epicenter is calibrated.

All accuracy codes in the C class are followed by the scale length XX (e.g. $CH_{90}02$).

Table 3.1. The C class accuracy codes. Parameters with asterisk are calibrated [38].

	Epicenter	**Focal Depth**	**Origin Time**
CH	*	*	*
CT	*		*
CF	*	*	
CE	*		

3.6.3. Network Geometry Criteria: The N Class

Events are considered as N class when the arrival time data is inadequate to establish the calibration process or the cluster is not applied with a form of calibration

technique yet. The accuracy codes for the N class can take 2 different forms:

- NE: "E" refers epicenter and only the epicenteral accuracy is evaluated by considering network geometry criteria.
- NF: "F" is for focal depth. Same as NE but focal depth is calibrated in addition.

All accuracy codes in the N class are followed by the scale length XX (e.g. $NF_{90}03$). It should be noted that events in this class are not considered as calibrated events, even in the NF case.

3.6.4. Uncalibrated Events: The U Class

Seismic events which cannot be classified with G, C or N categories are fell into the U Class, that is to say, it includes events with uncalibrated epicentral parameters.

3.6.5. Scale Length and Confidence Levels

Scale length represented as "XX" in the C and N Class accuracy codes is only linked to the uncertainty in epicenter. The scale length is evaluated by taking the nearest integer to the semi-major axis length of the confidence ellipse of an event and defined in kilometers.

All the confidence ellipses determined in mloc incorporates the uncertainties of the relative location and the calibration process with the 90% confidence level. It is very crucial to complement a scale length with the level of confidence in the subscript form (e.g. $CT_{90}5$) as suggested in Bondar et al. (2004) [41].

4. APPLICATION

4.1. Data Compilation

The process of relocating multiple events using mloc starts with gathering and preparing all the required data regarding the study area, in the region which includes the Salt Lake and its south-east respectively. The study has been conducted by using the data compiled from two different sources:

(i) First and foremost is the temporary CD-CAT network (YB). It is a very dense local seismic network containing 63 stations that is installed in Southern Anatolia (Figure 4.1), funded by National Science Foundation in order to investigate surface to mantle dynamics of Anatolia, Turkey [42]. The YB network had monitored seismic events occurred between 1th of June 2013 to 15th of May 2015 and it detected 10314 events (Figure 4.2). YB network plays an important role in the study owing its success on providing the near-distance phase readings needed for direct calibration technique.

(ii) Second source of data (including events within the same time-span as the former) is obtained from the online bulletin search tool of International Seismological Centre (ISC) [43]. Seismological agencies around the world supply data such as hypocentres, phase arrival-times, focal mechanism solutions etc. to the ISC and these data institute the bulletin of ISC. Earthquake Department of Disaster and Emergency Management Presidency (DDA) and Kandilli Observatory and Earthquake Research Institute (ISK) agencies are the ones that actively contributing seismological data to the ISC's bulletin from Turkey. Taking this into consideration and the mloc's ability to process merged bulletins put importance on the data obtained from the ISC bulletins in terms of decreasing azimuthal gap, along with supplying additional phase arrival-time information. In short, ISC online bulletin search tool is provided initial hypocentral locations, magnitudes and phase arrival-times of 5245 events recorded by 75 of ISK and 114 of DDA seismic stations (Figures 4.1 and 4.2).

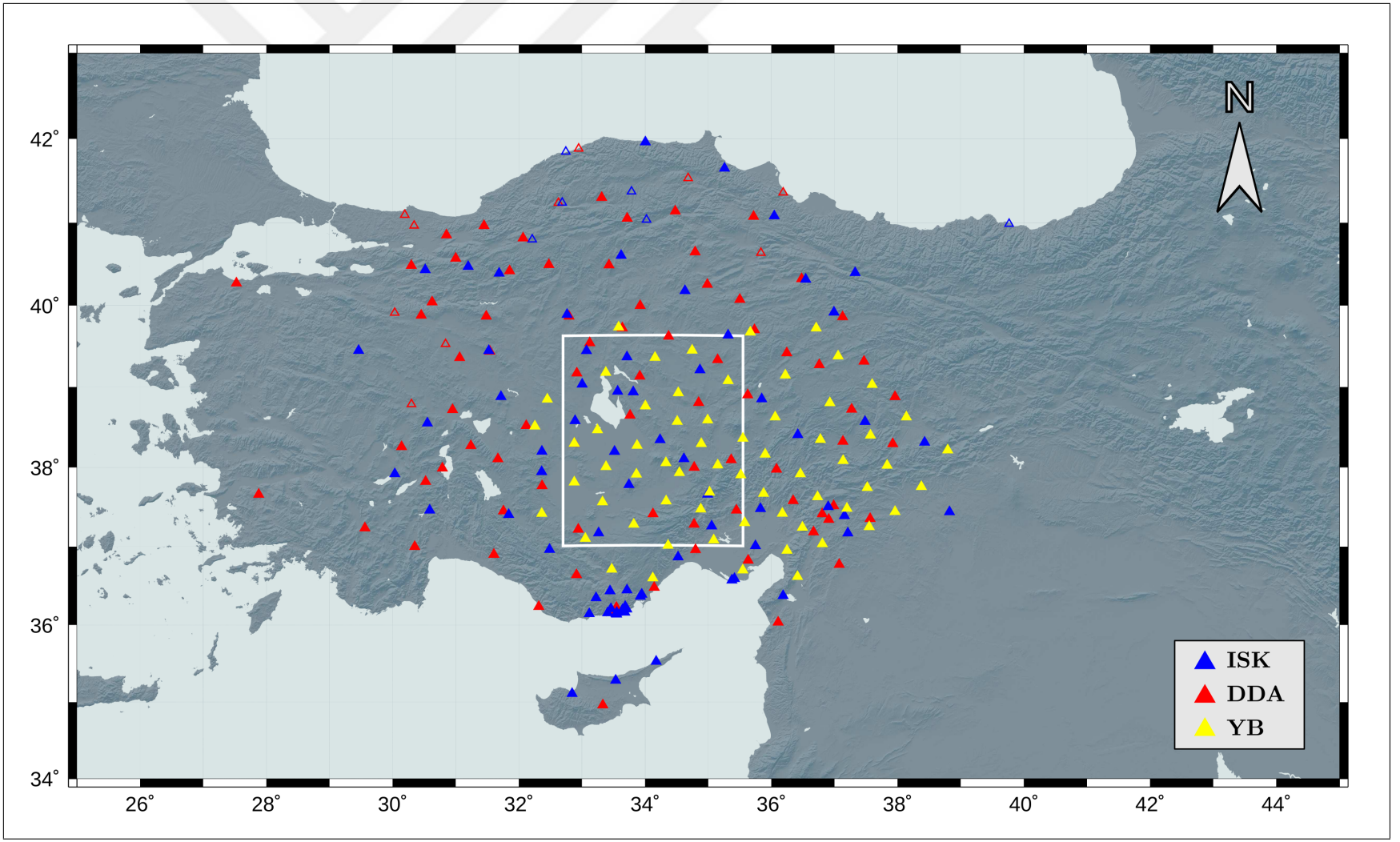

Figure 4.1. Map showing the study area and the stations used in the process. Each color represents different network. Empty triangles shows the stations which are only used at the start of the relocation procedure.

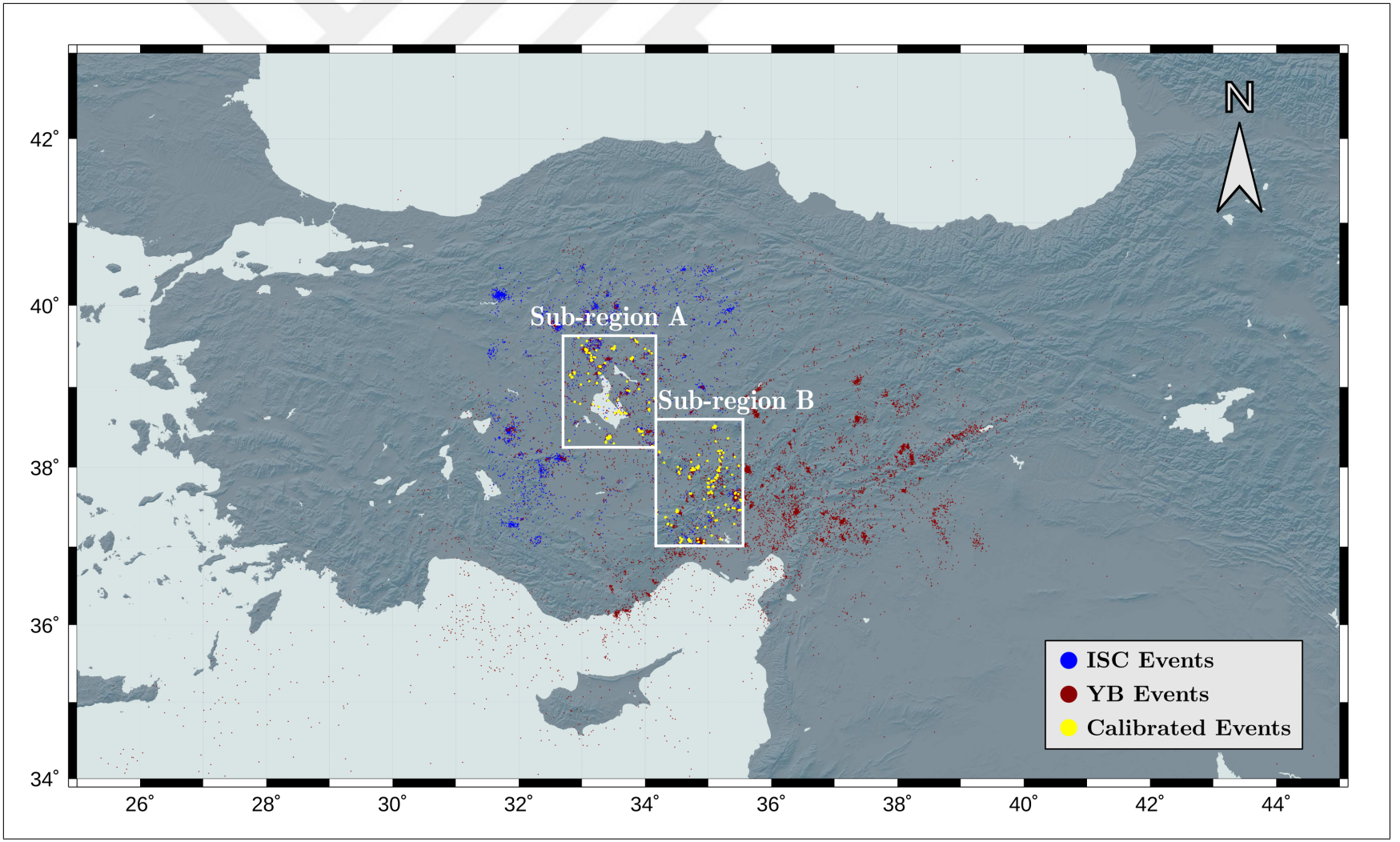

Figure 4.2. Map showing the events used in the study. Blue events are obtained from ISC, and, red events are obtained from CD-CAT Project. Yellow circles denotes relocated and calibrated events. White boundaries are the regional limits of the clusters.

4.2. Refining Bulletins

Both CD-CAT and ISC bulletins have been obtained in IMS1.0:short bulletin format and consequently they are converted into MNF bulletin format which is being used by the mloc program. Then, a script has been written to merge these two bulletins into one unified catalog appropriately. The most important aspect of the script is to determine identical events that are detected by both networks, in addition to this; list their reported initial locations, magnitude and depth information and phase arrival-time data under every corresponding event. Combining phase arrival-times of events that are recorded by different networks accompanied by various stations result in more accurate relocation results.

The large quantity of events as well as phase arrival-time data in the combined catalogue has made filtering the best recorded events possible. Therefore, the high quality catalogue has been exploited by only using the well recorded events containing 30 or more phase readings. Following that criteria, a search on the merged catalog provided the main bulletin with 495 events inside the study area. This, combined with the fact that the availability of near-distance seismic stations, make the direct calibration technique (Section 3.1) applicable in this study.

4.3. Determining Cluster Boundaries

As mentioned in the Section 3.3, the mloc program is able to relocate clusters up to 200 events within geographic extent of 100 kilometers or less. Two sub-regions; Sub-region A and Sub-region B have been created inside the study area by not only considering the ideal limits of mloc, but also reviewing the seismic activity, tectonic features, network coverage and data availability (Figure 4.2). Lastly, events which fall into the regional limits of those sub-regions have been separated and formed into two clusters (i.e. One cluster for each sub-region).

4.4. 1-D Velocity Model Assessment

Before initiating the relocation process on the newly formed clusters, it is expected to have an appropriate 1-D crustal velocity model that is coherent with the regarding region. Determination of the consistency between the theoretical 1-D velocity model and the medium inside the sub-region can be done by using a sub-cluster and estimating its spread of residuals in relation with the mean of residuals and inspecting the distribution of it for each phase type over assessed travel time model. This approach can yield accurate assumptions about the velocity model especially when a high quality sub-cluster (i.e. nearby events with good connectivity and high number of near-distance data) is created. Another advantage of working on preliminary sub-clusters is the ability to constrain an average depth for the sub-region and apply it during the main relocation process.

In the study, three layered 1-D crustal velocity models have been developed over the global average model ak135 [44] for the regions; Sub-region A (Table 5.2) and Sub-region B (Table 5.4), by adjusting layer depths and velocities to fit P and S wave arrival time data.

Up until this point, all the steps shown are carried out for establishing a strong foundation to the relocation study. Compilation and refinement of the bulletins, determination of the regional limits, choosing an appropriate calibration technique, assessment of 1-D velocity model and average depth of sub-regions were the systematical measures has been taken to initiate the relocation process.

4.5. Relocating Clusters

Relocation process in mloc is based on improving the solutions each run by identifying the different types of uncertainty and helping user to clean out the outliers manually. Outlier removal procedure which is explained thoroughly in the Section 3.4 is used in this process.

After the relocation procedure, the program outputs the relocation results, including the solutions of epicentral parameters and estimated uncertainties along with the other statistical data calculated during the algorithm after each consecutive run. Improved relocation solutions basically rely on the evaluation of these output in between runs.

Two clusters situated within the study area have been relocated by using the predetermined 1-D crustal velocity models and fixed average cluster depths. Relocation solutions have been calibrated using the direct calibration technique (Section 3.1) due to abundance of the near-distance data and lack of ground truth events needed for indirect calibration. Relocation results and further statistical data have been mapped and plotted using the Generic Mapping Tools (GMT v5.3.1) [45–48]. The Flow chart showing the stages of the relocation process is given in Figure 4.3.

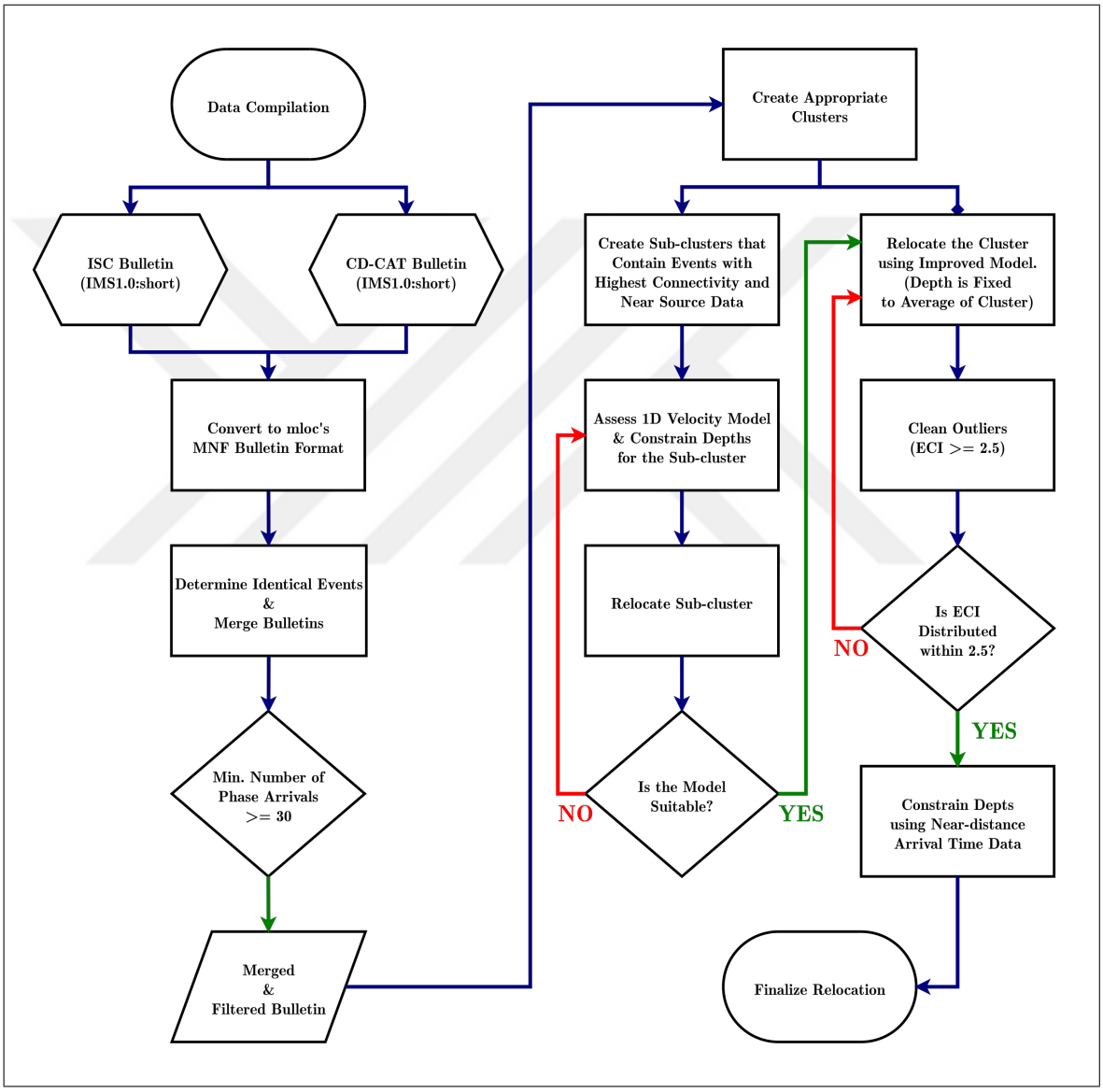

Figure 4.3. Flow chart showing the workflow followed in the study.

4.6. Determining Depths

After the epicentral parameter relocation is applied, the depth of each event in the clusters is constrained, and evaluated whenever necessary depth related data are available. Direct P_g phase arrivals from very near distance have been exploited to determine the depths. The general rule of thumb when deciding if a near source data can be considered as near-distance is making sure the epicentral distance between the event and the station is not more than double amount of the evaluated depth [49]. For example, in a case where depth of an event is being evaluated as 5 kilometers using the phase arrival time from the nearest station, maximum of 10 kilometers distance between that station and the event is considered as a near-distance station. In other cases when there are no near-distance data, depth determination can be done by using local-distance data. However, it should be kept in mind that the evaluation might not be as accurate as using very near-distance data.

Determination of the depth is done by tracking the slight changes of the residuals on the near-distance phase arrivals after each run for an assumed depth. For instance, a negative residual on the nearest phase arrival would mean that observation falls short of the theoretical prediction time. This can be compensated by moving the source closer to the recording station. Meaning, the depth should be set shallower than the first evaluation. Following the same analogy, a positive residual can be handled by moving assumed depth to a deeper position. Evaluation of depth for each event continues until near-distance phase arrival residuals are close to zero, and, the farther readings positive and negative residuals are reach to an equilibrium.

5. RESULTS

A total of 394 events, each having more than 30 phase arrivals were found to be situated within the main interest regions; Sub-region A and Sub-region B (Figure 5.1). Therefore, have been used to initiate relocation process by using their initial locations and phase arrival time data as explained thoroughly in the Sections 3.3 and 4.2. As a result, 298 out of 394 events have been successfully relocated and calibrated which is done by applying direct calibration technique (Section 3.1). Furthermore, by considering details mentioned in the Section 4.6, depth information of 243 events have been determined by using the near-distance or local distance phase readings. Statistics of events relocated, calibrated and depths determined for each sub-region is given in the Table 5.1 in detail.

Table 5.1. Table showing the amount of events relocated, calibrated and depths determined in the study.

Region	**All Events (No. of Phase Arrivals ≥30)**	**Relocated and Calibrated**	**Removed from Final Catalogue**	**Depths Determined Using the Readings from:**		**Fixed Depth**
				Near Distance	**Local Distance**	
Sub-region A	194	137	12	73	49	3
Sub-region B	200	163	2	80	41	40
Total	394	300	14	153	90	43

Events removed from the catalog after relocation consists of:

(i) Events that are suspected for mining explosions. These type of events identified after a depth assessment. Explosion events detected in the main interest regions tended to give out depths very near or above the surface level.

(ii) Events which have connectivity issues resulting with greater uncertainties compared to other solutions.

Relocation solutions of events for each interest regions are shown in Figure 5.1. Results of the study will be investigated in-depth under following subsections.

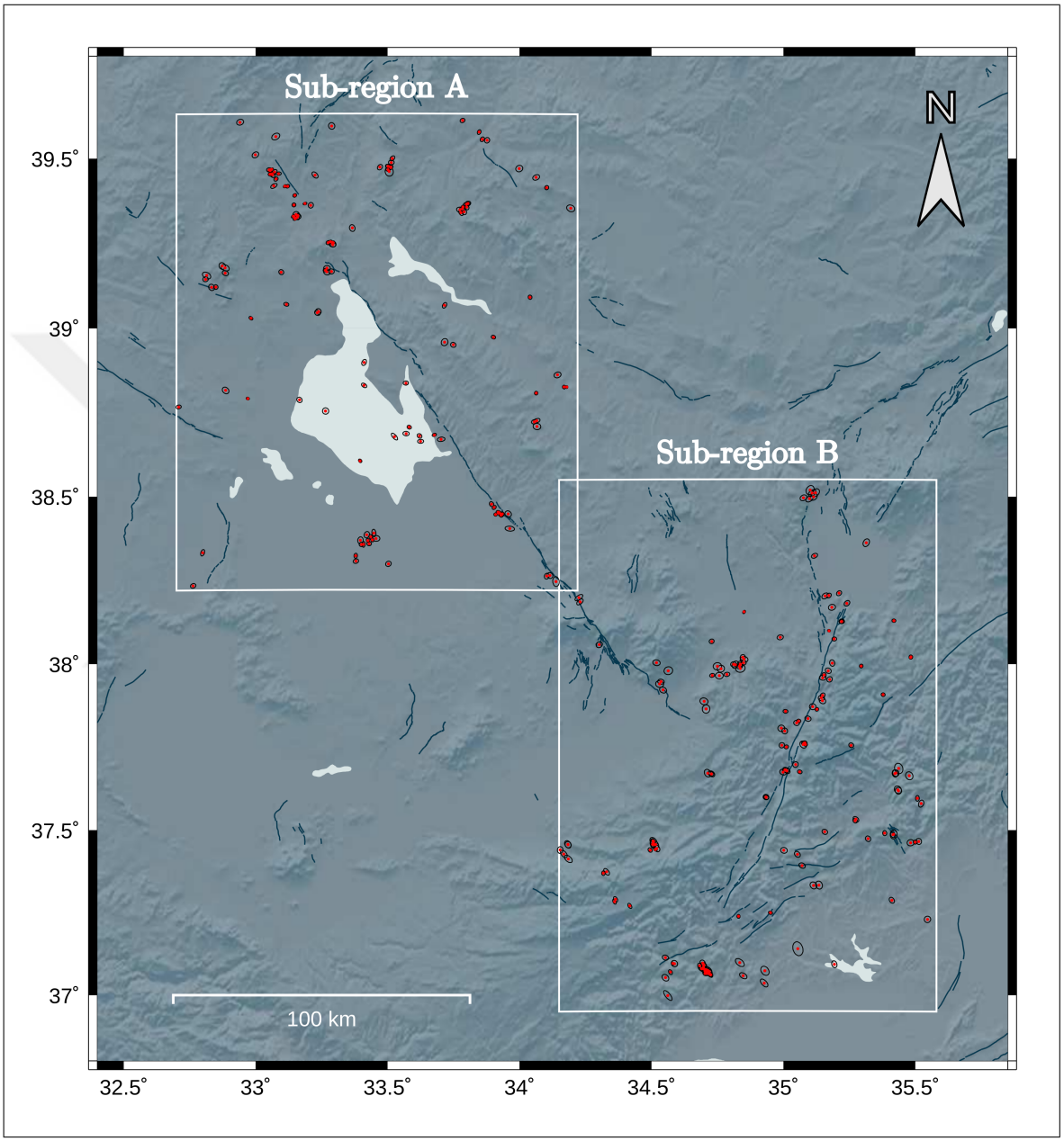

Figure 5.1. Overview of the relocation results for Sub-region A and Sub-region B. Red circles denote the epicenter of relocated events and ellipses with black lines shows the estimated uncertainties for each event with 90% confidence. Detailed map of each Sub-region are illustrated in the Figures 5.6 and 5.11.

5.1. Analysis of Sub-region A

The cluster residing within the Sub-region B is centered around Salt Lake, Anatolia which includes the seismic activity from the Salt Lake Fault Zone (SLFZ). 137 earthquakes have been relocated and calibrated using the 1-D velocity model that was especially crafted for the region (Table 5.2 and Figure 5.2).

Table 5.2. The crustal velocity model determined and used in the relocation of earthquakes in the Sub-region A.

Depth to Top Layer (km)	P Velocity (km/s)	S velocity (km/s)
0	5.5	3.375
6	6.0	3.475
11	6.5	3.6
36	7.95	4.6

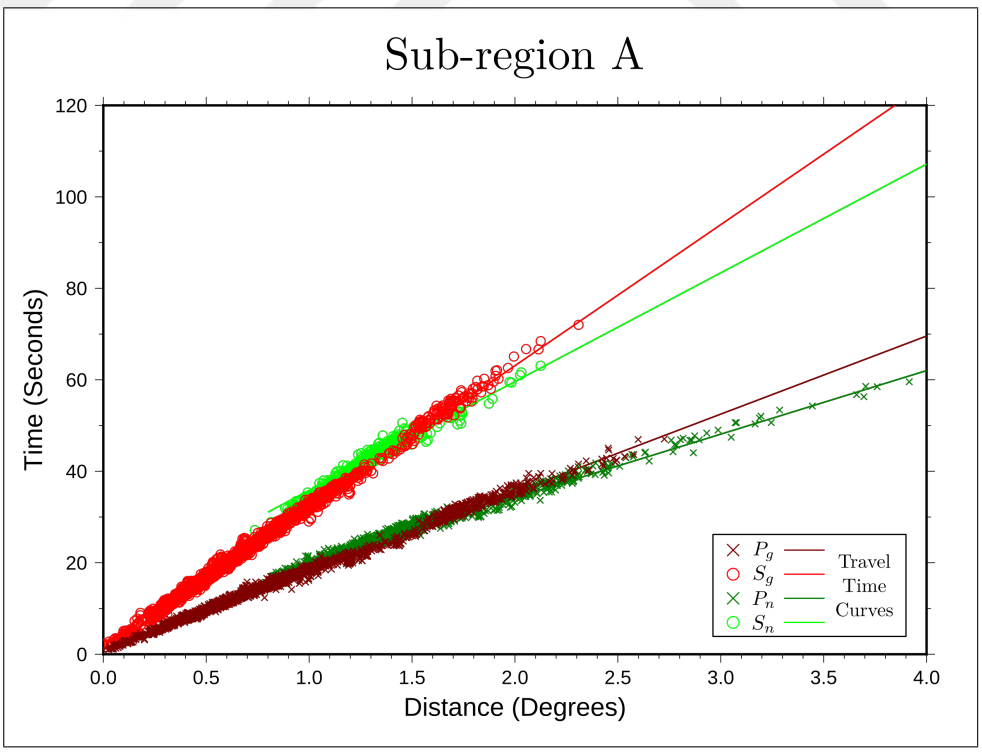

Figure 5.2. Crustal phase arrival times of the earthquakes against the travel time curves of Sub-region A.

A total number of 2431 and 7066 readings have been used to determine hypocentroid and cluster vectors, respectively. Determination of the hypocentroid as well as the application of direct calibration technique have been done by using the 2431 short distance readings ($< 0.7°$) which is shown in Figure 5.3.

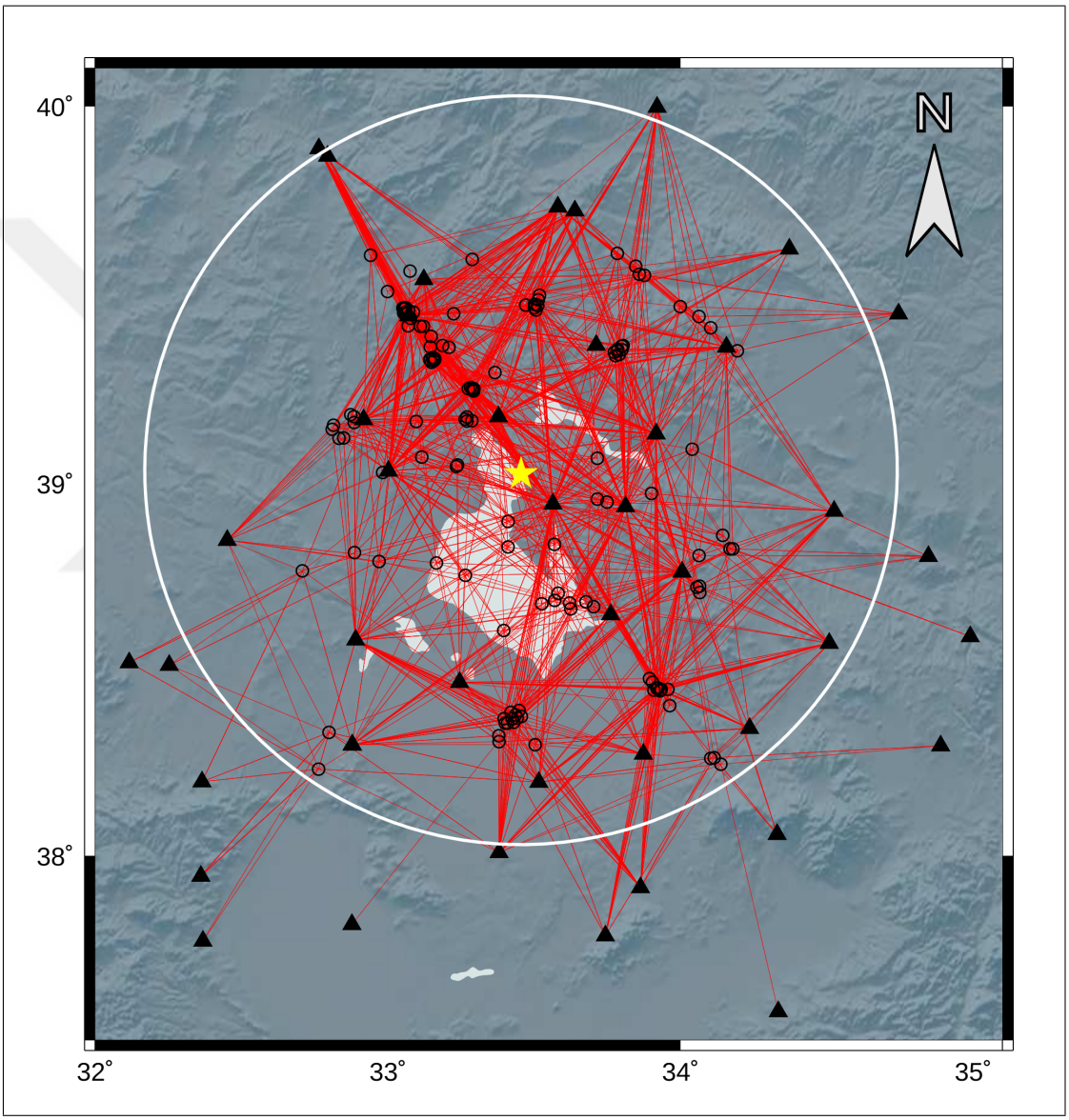

Figure 5.3. Ray paths (red lines) used to locate hypocentroid of the Sub-region A. Triangles are stations and open circles are events used in the direct calibration process. Yellow star denotes the hypocentroid of the cluster and open white circle is centered at the hypocentroid with 1° radius as a scale.

The definition and determination of the "Empirical Path Anomaly" and "Spread" is widely explained in the Section 3.4. When evaluated together, these parameters can be informative on delivering the consistency of phase readings for each station against the travel time model used for the region. In most cases, nonuniform nature of the empirical path anomalies and spread throughout the region stem from the lack of detail 1-D velocity models carries into the location problem, as it is highly unreasonable to represent all the distinctive geological formations, layering and seismic anisotropy only with a 1-D velocity model. Another reason for such discrepancies would be the random picking errors, although it can be eliminated by increasing the sample size as it has been done on this study.

Empirical path anomaly over spread plots for P_g and S_g phases have been made within the geographic extent of 2° centered at the hypocentroid for each station having 2 or more station phase readings for the events occurred in the Sub-region A.

Map of empirical path anomaly over spread for the P_g phase has been shown in Figure 5.4. According to the map, empirical path anomaly and spread estimations seems coherent within the 1° radius circle other than the stations AT41 and SULT where residuals about +0.45 seconds is observed. Estimated spread on these stations average on +0.22 seconds which makes the readings consistent. This information might lead to a conclusion about the slower than average velocity structure near these stations, as positive residuals indicates P_g phase arrivals observed later than they should be [50]. Similar analogy can be made for the other distant stations ($1° < D < 1.6°$ to the hypocentroid), however, systematic errors related with the velocity model increases with the distance as discussed above.

Map of empirical path anomaly over spread for the S_g phase has been shown in Figure 5.5. Same case as in the Figure 5.4 where velocity structure thought to be slower than the rest in the southern part of the Salt Lake is also observed with the S_g station phase readings of AT41, SULT as well as AT42 in addition.

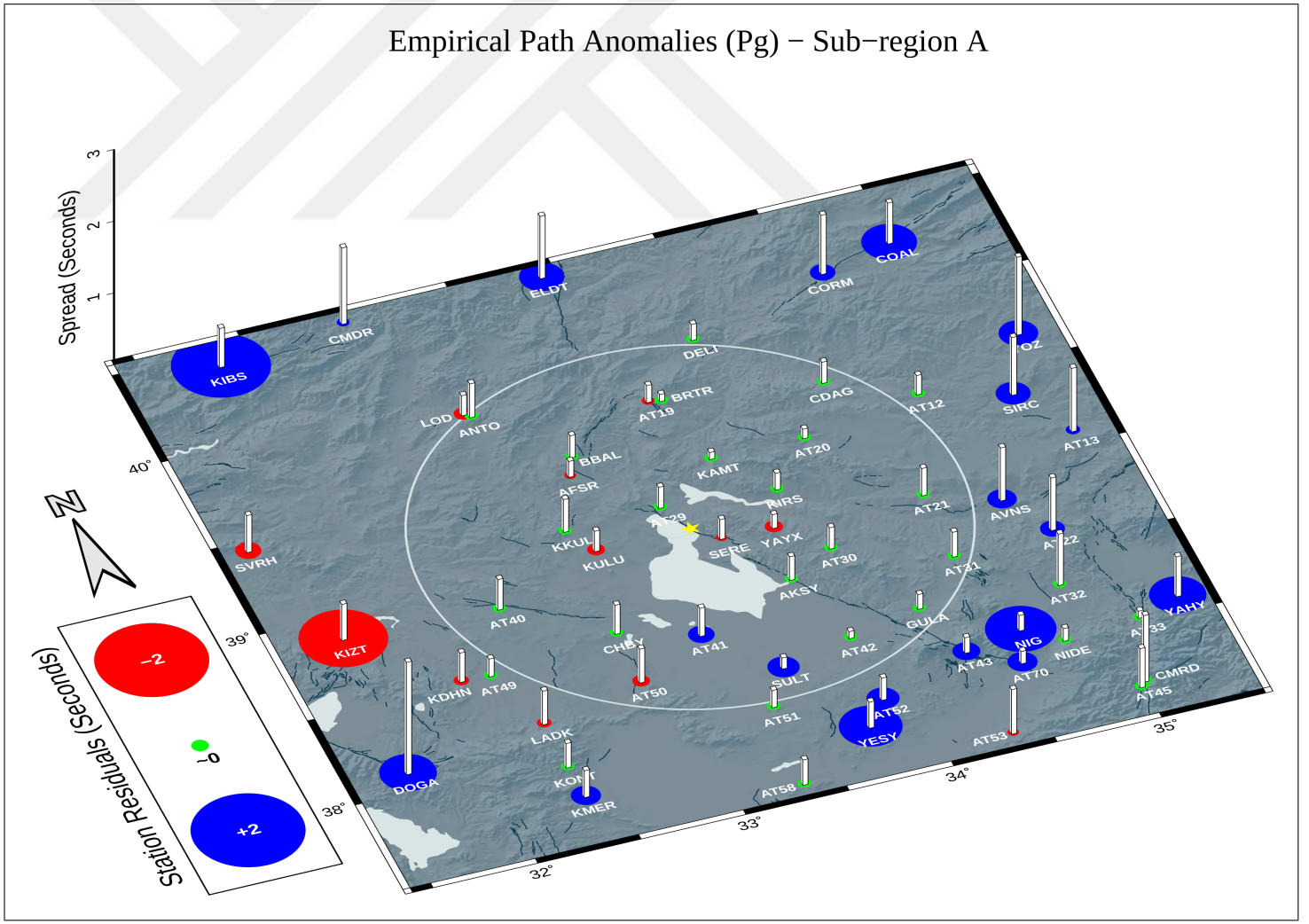

Figure 5.4. Map of empirical path anomaly over spread for the observed P_g station phases for the earthquakes occurred in the Sub-region A. Yellow star denotes the hypocentroid.

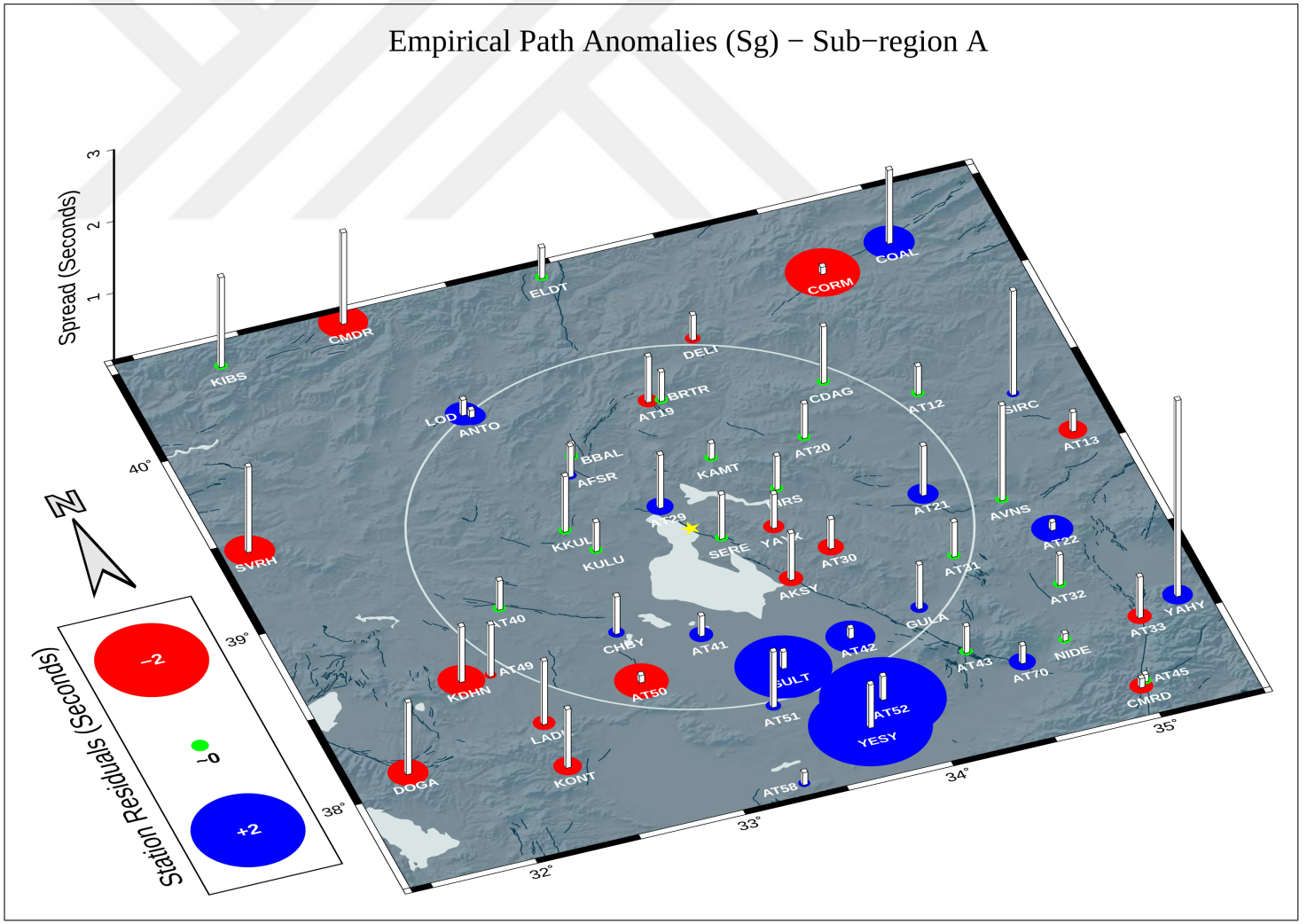

Figure 5.5. Map of empirical path anomaly over spread for the observed S_g station phases for the earthquakes occurred in the Sub-region A. Yellow star denotes the hypocentroid.

Magnitudes reported by ISC and CD-CAT networks for the events relocated in the Sub-region A range from local magnitude (ML) of 1 and 3.5. Average of the azimuthal gap for determining cluster vectors is found to be 53.9 degrees. Error ellipses with 90% confidence representing the uncertainties in the location of each event have been estimated, thus, larger semi-axes of the error ellipses observed to vary between 1 and 1.8 kilometers. Furthermore, event with the lowest estimated uncertainty (Event #5) has the minor and major semi-axes length of 0.7 km and 0.9 km respectively. The area of the error ellipse of this event is 2.4 km^2. Event with the highest uncertainty (Event #104) has the minor and major semi-axes length of 1.2 km and 1.6 km respectively. The area of the error ellipse of this event is 6.6 km^2.

Results of the 12 events out of 137 have been removed from the final catalogue; 10 of which suspected as mining explosions and 2 found to have connectivity issues with the cluster.

The resulting catalogue constitutes calibrated locations of 125 events. Focal depths of these events are constrained and average depth of the cluster determined as 5.6 kilometers. Focal depth of 73 earthquakes have been determined by using the near distance readings ($< 0.2°$) with the estimated error of $\sim$2 kilometers. Moreover, focal depths of 49 events have been determined by using the local distance readings with the estimated error of $\sim$4 kilometers. The rest of the 3 events have been fixed to the average depth of the cluster (Figure 5.6).

Map of the relocation results along with the depth cross-section for the Sub-region A is shown in the Figure 5.6. Statistics of each relocated and calibrated event is listed in the Table 5.3.

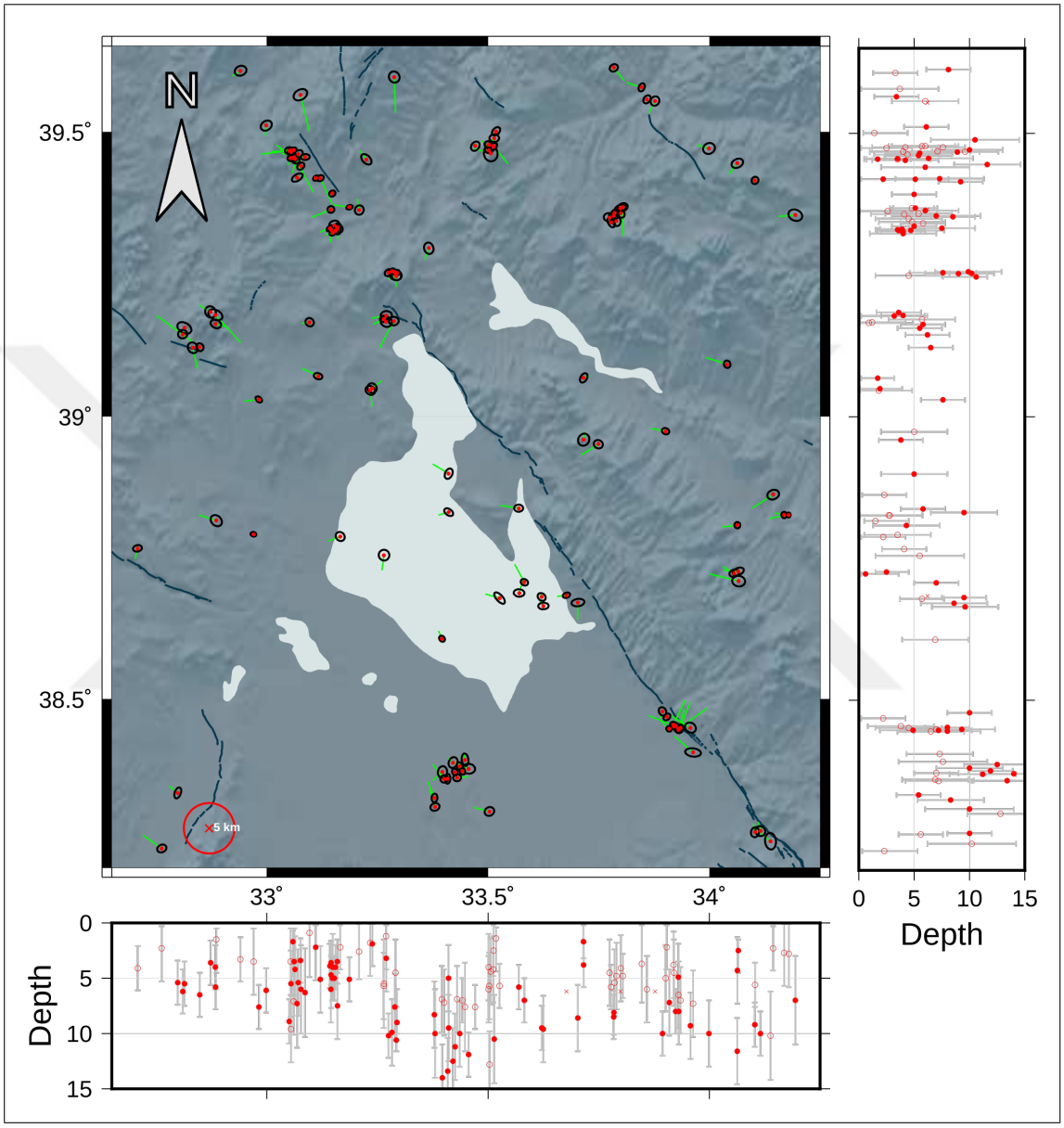

Figure 5.6. Epicenters and depths of earthquakes relocated in the Sub-region A. Map: Red dots are locations and ellipses are for relative location with 90% confidence. Green lines shows the change from the initial single-event location. Open red circle of 5 km radius is shown as a scale. Cross-section: Closed and open red circles are depths determined by near and local distance readings, respectively. Fixed depths marked with an "x". Gray bars are estimates of error on depths.

Table 5.3. Statistics of the earthquakes relocated and calibrated within the Sub-region A. Origin time is given in GMT. Parameters of 90% confidence ellipses are defined as following: AZ1 and AZ2 shows the azimuths of elliptical semi-axes, and, L1 and L2 represents the corresponding lenghts of semi-axes. Area of the confidence ellipses are given in the "Area (km^2)" column. Accuracy codes are defined in the last column. Classification has been done using the procedures explained in Section 3.6.

Event Number	Date	Time	Latitude	Longitude	Depth (km)	Magnitude	Type	AZ1	L1	AZ2	L2	Area (km^2)	GCNU Code
1	2013/06/12	02:18:50.29	39.34966	33.77436	4.5	2.1	ML	357	1.07	87	1.41	4.7	CH01
2	2013/06/18	16:25:27.12	39.41998	33.06856	7.3	2.2	ML	332	0.88	62	1.48	4.1	CH01
3	2013/06/25	05:00:41.06	39.4684	33.06102	7.1	2.1	ML	337	0.77	67	1.09	2.6	CH01
4	2013/06/25	14:08:41.25	38.82634	34.16869	2.7	2.5	ML	340	0.87	70	1.08	3	CH01
5	2013/06/25	15:37:48.70	38.826	34.17925	2.8	2.6	ML	339	0.77	69	0.99	2.4	CH01
6	2013/06/25	21:54:03.34	39.46688	33.05072	8.9	2	ML	347	0.92	77	1.24	3.6	CH01
7	2013/06/28	19:30:49.13	39.122	32.84875	6.5	3	ML	344	0.99	74	1.15	3.6	CH01
8	2013/07/08	01:39:21.16	39.35814	33.78546	5.4	2.5	ML	330	0.82	60	1.14	2.9	CH01
9	2013/07/08	20:07:12.62	39.35443	34.19408	7	2	ML	9	1.28	99	1.62	6.5	CH02
10	2013/07/11	19:50:55.37	39.35749	33.79999	4.1	2.8	ML	358	1.04	88	1.15	3.7	CH01
11	2013/07/23	04:37:05.77	38.35817	33.40882	13.4	2	ML	297	0.98	27	1.2	3.7	CH01
12	2013/08/10	11:56:13.84	38.36001	33.42995	6.9	3.1	ML	345	0.93	75	1.2	3.5	CH01
13	2013/08/10	18:10:21.89	39.46775	33.05502	9.6	2.7	ML	339	0.76	69	1.09	2.6	CH01
14	2013/08/11	23:16:10.35	38.47786	33.89395	10	1.8	ML	353	1.04	83	1.16	3.8	CH01
15	2013/08/12	00:35:00.55	38.3867	33.42073	12.5	1.6	ML	317	1.12	47	1.37	4.8	CH01
16	2013/08/12	01:14:19.00	38.39169	33.44762	7.6	1.8	ML	270	1.11	0	1.39	4.9	CH01
17	2013/08/13	20:11:23.72	38.3704	33.39671	14	1.8	ML	304	1.22	34	1.38	5.3	CH01
18	2013/08/14	01:19:10.35	38.37161	33.44202	7	1.9	ML	338	0.96	68	1.05	3.2	CH01
19	2013/08/14	01:46:04.72	38.35766	33.401	7.2	1.8	ML	343	0.96	73	1.2	3.6	CH01
20	2013/08/15	18:57:44.85	38.36956	33.42539	11.2	2.7	ML	347	0.92	77	1.05	3	CH01
21	2013/08/26	05:37:14.32	38.38045	33.43598	10	2.4	ML	25	1.07	115	1.07	3.6	CH01
22	2013/08/26	22:06:33.75	38.37553	33.45598	11.9	1.7	ML	356	1.16	86	1.56	5.7	CH02
23	2013/08/27	15:14:42.59	38.72613	34.06538	2.5	2.1	ML	338	0.92	68	1.48	4.3	CH01
24	2013/08/28	01:47:56.08	39.36283	33.20851	2.6	1.5	ML	332	1.08	62	1.27	4.3	CH01

Event Number	Date	Time	Latitude	Longitude	Depth (km)	Magnitude	Type	AZ1	L1	AZ2	L2	Area (km^2)	GCNU Code
25	2013/08/28	04:06:30.32	38.40522	33.96305	7.3	2.1	ML	2	1.05	92	1.79	5.9	CH02
26	2013/08/29	03:03:18.87	39.47087	33.9989	10	2	ML	338	1.2	68	1.49	5.6	CH01
27	2013/08/29	17:54:29.51	38.68111	33.62126	9.5	1.8	ML	360	1	90	1.19	3.7	CH01
28	2013/09/10	11:35:08.62	38.26333	34.103	5.6	2.2	ML	318	1.09	48	1.28	4.4	CH01
29	2013/09/19	20:10:44.53	39.4451	34.06281	11.6	1.8	ML	337	1.03	67	1.5	4.8	CH01
30	2013/10/10	21:15:36.12	39.45243	33.06396	4.2	2.1	ML	5	1.04	95	1.23	4	CH01
31	2013/10/13	19:03:45.43	39.25416	33.2893	7.6	2.6	ML	347	0.8	77	1.06	2.6	CH01
32	2013/10/19	17:55:42.63	39.24682	33.29275	10.6	1.9	ML	351	1.01	81	1.27	4	CH01
33	2013/10/19	19:21:21.26	39.24908	33.29074	4.5	2	ML	2	1.21	92	1.49	5.6	CH01
34	2013/10/21	03:50:05.36	39.46097	33.07124	5.4	1.8	ML	333	0.92	63	1.33	3.8	CH01
35	2013/10/22	16:05:56.16	39.44025	33.07743	6	2.7	ML	331	0.87	61	1.19	3.2	CH01
36	2013/10/22	23:58:03.13	39.25261	33.29432	9	2.9	ML	337	0.8	67	1.07	2.7	CH01
37	2013/10/25	11:16:29.27	38.81642	32.88609	1.5	2.1	ML	20	1.25	110	1.44	5.6	CH01
38	2013/10/29	11:27:38.00	39.25581	33.2829	9.9	3.1	ML	339	0.76	69	1.1	2.6	CH01
39	2013/10/29	11:57:15.32	39.25295	33.2751	10.2	1.9	ML	334	0.87	64	1.19	3.3	CH01
40	2013/11/21	02:11:32.92	39.34127	33.77788	5.8	1.8	ML	39	1.05	129	1.21	4	CH01
41	2013/11/29	23:29:51.20	39.32853	33.14517	3.6	2.1	ML	343	0.78	73	1.04	2.5	CH01
42	2013/11/30	01:28:08.43	39.32891	33.14539	4.7	1.7	ML	344	0.8	74	1.05	2.6	CH01
43	2013/12/09	04:34:53.78	39.45448	33.05901	1.7	3	ML	342	0.79	72	1.07	2.6	CH01
44	2013/12/17	21:24:01.48	39.55671	33.85896	6	2	ML	327	0.91	57	1.22	3.5	CH01
45	2013/12/21	14:46:13.47	38.7228	34.05605	0.6	2.2	ML	342	0.93	72	1.32	3.9	CH01
46	2013/12/23	21:57:56.48	39.34381	33.78991	4.8	1.8	ML	334	1.18	64	1.21	4.5	CH01
47	2013/12/28	17:38:50.47	39.32668	33.15562	4	2.2	ML	7	0.96	97	1.28	3.9	CH01
48	2014/01/03	12:18:33.15	39.33002	33.15966	3.5	2.1	ML	351	1.04	81	1.35	4.4	CH01
49	2014/01/07	12:39:26.77	39.47738	33.50126	6	2.1	ML	360	0.98	90	1.18	3.6	CH01
50	2014/01/13	00:26:10.44	39.55402	33.87711	6.2	1.6	ML	331	1.06	61	1.28	4.2	CT01
51	2014/01/13	10:33:19.27	39.16571	33.09657	0.9	2.4	ML	350	1.04	80	1.21	3.9	CH01
52	2014/02/02	17:44:24.48	38.8083	34.06313	4.3	2.2	ML	340	0.86	70	1.08	2.9	CH01
53	2014/02/04	20:54:41.65	39.32324	33.14925	4	2	ML	339	0.77	69	1.13	2.7	CH01
54	2014/02/06	04:11:00.81	39.57832	33.84733	3.7	2.1	ML	321	0.91	51	1.17	3.3	CH01

Event Number	Date	Time	Latitude	Longitude	Depth (km)	Magnitude	Type	AZ1	L1	AZ2	L2	Area (km^2)	GCNU Code
55	2014/02/06	23:28:20.22	39.33097	33.1426	3.9	1.7	ML	333	0.77	63	1.19	2.9	CH01
56	2014/02/07	18:22:27.27	38.33295	32.79884	5.4	1.7	ML	305	0.98	35	1.37	4.2	CH01
57	2014/02/08	16:53:39.17	39.36817	33.18667	5.1	2.2	ML	342	0.73	72	1.12	2.6	CH01
58	2014/02/14	03:48:28.47	39.33609	33.15279	5	1.8	ML	341	1.12	71	1.39	4.9	CH01
59	2014/02/21	08:51:55.05	38.46825	33.90352	2.2	2	ML	332	0.84	62	1.18	3.1	CH01
60	2014/02/27	03:09:03.80	39.16291	32.88452	5.8	1.9	ML	4	1.05	94	1.35	4.5	CH01
61	2014/03/23	18:41:19.45	39.02989	32.98228	7.6	2	ML	1	0.87	91	1.09	3	CH01
62	2014/03/26	12:58:30.00	39.46769	33.50141	4	2.2	ML	357	0.89	87	1.15	3.2	CH01
63	2014/03/27	21:34:11.17	39.46509	33.05476	5.5	1.7	ML	346	0.75	76	1.15	2.7	CH01
64	2014/04/03	07:07:44.36	39.41469	34.10264	9.2	1.8	ML	336	0.91	66	1.15	3.3	CH01
65	2014/04/05	06:04:50.27	38.83753	33.56934	5.8	2	ML	348	0.94	78	1.26	3.7	CH01
66	2014/04/07	06:40:57.37	38.26522	34.11514	10	2.1	ML	354	1.18	84	1.33	4.9	CH01
67	2014/04/07	20:09:32.55	38.78787	33.16608	2.2	2	ML	356	1.1	86	1.25	4.3	CH01
68	2014/04/09	04:13:07.63	38.30811	33.38028	10	2.4	ML	341	0.95	71	1.3	3.9	CH01
69	2014/04/27	01:34:26.82	38.79171	32.97038	3.5	2.4	ML	348	0.77	78	1.06	2.6	CH01
70	2014/05/04	23:15:35.55	38.89906	33.4107	5	1.2	ML	314	1.02	44	1.34	4.3	CH01
71	2014/05/06	11:39:31.41	39.47544	33.51171	4.2	1.9	ML	328	0.86	58	1.19	3.2	CH01
72	2014/05/11	01:49:36.60	38.66483	33.62472	9.6	1.8	ML	351	0.9	81	1.36	3.9	CH01
73	2014/05/22	16:42:22.00	38.95903	33.71585	3.8	1.7	ML	323	1.27	53	1.49	6	CH01
74	2014/05/28	11:21:12.75	39.47392	33.51217	2.5	1.6	ML	325	0.86	55	1.25	3.4	CH01
75	2014/05/30	05:14:21.80	39.41925	33.11068	2.2	2.2	ML	336	0.77	66	1.1	2.6	CH01
76	2014/06/06	13:23:36.88	39.50058	33.51793	1.4	1.9	ML	327	0.9	57	1.3	3.7	CH01
77	2014/06/14	13:45:29.98	38.3241	33.37875	8.3	2.2	ML	316	0.97	46	1.14	3.5	CH01
78	2014/06/27	12:45:02.47	39.47725	33.50287	5.7	2	ML	356	0.99	86	1.24	3.9	CH01
79	2014/07/07	09:38:29.57	38.75478	33.26463	5.5	1.6	ML	342	1.22	72	1.38	5.3	CH01
80	2014/07/15	23:37:17.80	38.97359	33.90125	5	2.1	ML	353	0.89	83	1.15	3.2	CH01
81	2014/07/22	20:52:15.19	39.45582	33.08664	6.3	1.8	ML	348	0.83	78	1.25	3.3	CH01
82	2014/07/28	18:31:53.70	38.23397	32.76271	2.3	2.2	ML	339	0.96	69	1.31	3.9	CH01
83	2014/08/12	12:02:05.19	39.45412	33.05409	3.5	2.6	ML	343	0.83	73	1.1	2.9	CH01
84	2014/08/12	14:13:28.32	38.60666	33.39556	6.9	2	ML	351	0.88	81	1.06	2.9	CH01

Event Number	Date	Time	Latitude	Longitude	Depth (km)	Magnitude	Type	AZ1	L1	AZ2	L2	Area (km^2)	GCNU Code
85	2014/08/21	16:00:54.54	39.45544	33.06205	3.5	2.5	ML	334	0.97	64	1.14	3.5	CH01
86	2014/08/27	16:40:54.35	39.36373	33.14509	6	2.4	ML	341	0.89	71	1.13	3.2	CH01
87	2014/09/12	03:08:38.18	39.17859	32.88391	4	1.9	ML	16	1.2	106	1.66	6.3	CH02
88	2014/09/23	01:51:47.20	39.17159	33.26448	5.7	2.1	ML	339	0.85	69	1.17	3.1	CH01
89	2014/09/23	04:07:27.34	39.17775	33.26997	3.2	1.8	ML	348	1.04	78	1.42	4.6	CH01
90	2014/09/23	15:50:32.68	39.16665	33.26959	1.2	2.2	ML	2	1.22	92	1.42	5.4	CH01
91	2014/10/16	10:24:55.27	39.60653	32.94057	3.3	2.2	ML	340	1.11	70	1.49	5.2	CH01
92	2014/10/27	16:34:30.50	39.56462	33.07629	3.4	1.8	ML	333	1.16	63	1.68	6.1	CH02
93	2014/10/28	19:33:35.25	38.7666	32.70849	4.1	2.4	ML	344	0.88	74	1.27	3.5	CH01
94	2014/11/28	12:48:11.09	39.48856	33.51384	10.5	1.9	ML	349	0.97	79	1.3	3.9	CH01
95	2014/12/02	21:55:34.13	38.86235	34.14392	2.3	1.8	ML	340	1.1	70	1.49	5.2	CH01
96	2014/12/04	20:57:32.80	38.67097	33.7027	8.6	1.5	ML	349	0.95	79	1.56	4.7	CH02
97	2014/12/05	00:08:34.85	39.51132	32.9987	6.1	1.6	ML	333	1.08	63	1.47	5	CH01
98	2014/12/20	01:39:46.83	38.29969	33.50328	12.8	1.4	ML	338	1.04	68	1.33	4.3	CH01
99	2015/01/04	15:57:21.37	39.33268	33.15974	7.5	2.1	ML	339	0.93	69	1.18	3.4	CH01
100	2015/01/11	06:33:37.59	39.39238	33.14823	5	2.4	ML	337	0.83	67	1.12	2.9	CH01
101	2015/01/15	10:02:43.08	38.44705	33.90935	7.2	2.3	ML	344	0.83	74	1.07	2.8	CH01
102	2015/01/17	03:31:30.91	39.41896	33.12086	5.1	2	ML	338	0.82	68	1.15	3	CH01
103	2015/01/18	21:21:51.91	39.14459	32.81023	6.2	1.8	ML	344	1.03	74	1.28	4.2	CH01
104	2015/01/18	23:44:59.70	39.15628	32.81443	5.5	1.6	ML	20	1.24	110	1.68	6.6	CH02
105	2015/01/19	03:30:19.02	38.44874	33.93447	7	1.6	ML	347	0.92	77	1.11	3.2	CH01
106	2015/01/19	04:50:41.10	38.4472	33.92966	4.9	1.7	ML	346	0.88	76	1.21	3.3	CH01
107	2015/01/20	13:27:02.71	38.45114	33.91982	4.5	3.5	MW	342	0.77	72	1.03	2.5	CH01
108	2015/01/20	14:01:42.01	38.44874	33.95705	9.3	1.8	ML	5	1.2	95	1.4	5.3	CH01
109	2015/01/20	19:59:25.05	38.44555	33.93097	8	2	ML	329	0.95	59	1.13	3.4	CH01
110	2015/01/20	20:56:10.98	38.45428	33.91903	3.8	1.7	ML	349	0.87	79	1.15	3.1	CH01
111	2015/01/21	10:55:57.07	38.44509	33.92996	6.5	2.1	ML	355	0.84	85	1.18	3.1	CH01
112	2015/01/27	03:52:17.11	38.70708	33.58191	7	1.8	ML	352	0.9	82	1.15	3.3	CH01
113	2015/01/28	00:03:14.79	39.18407	32.87318	3.6	1.8	ML	2	1.29	92	1.37	5.5	CH01
114	2015/01/28	02:39:50.77	38.67887	33.526	5.7	2.1	ML	41	1.06	131	1.56	5.2	CH02

Event Number	Date	Time	Latitude	Longitude	Depth (km)	Magnitude	Type	AZ1	L1	AZ2	L2	Area (km^2)	GCNU Code
115	2015/02/05	06:43:03.79	39.36589	33.79895	6.2	2.2	ML	340	0.9	70	1.47	4.1	CT01
116	2015/02/07	08:05:23.42	39.36806	33.8043	4.8	2.4	ML	340	0.97	70	1.35	4.1	CH01
117	2015/02/16	07:37:26.35	39.6125	33.78424	8.1	1.9	ML	338	0.92	68	1.23	3.6	CH01
118	2015/02/16	16:44:14.41	39.35296	33.78368	8.5	1	ML	336	0.99	66	1.38	4.3	CH01
119	2015/02/16	19:49:29.55	38.4521	33.92378	8	1.3	ML	355	0.91	85	1.12	3.2	CH01
120	2015/03/10	11:38:17.65	39.47543	33.47075	7.6	2.2	ML	325	1	55	1.31	4.1	CH01
121	2015/04/06	23:32:00.09	38.83112	33.41085	9.5	1.8	ML	13	0.98	103	1.25	3.8	CH01
122	2015/04/11	15:23:08.36	38.68354	33.67714	6.2	2.8	ML	340	0.78	70	1.18	2.9	CT01
123	2015/04/19	17:38:11.31	39.06804	33.71553	1.7	2.2	ML	317	0.95	47	1.3	3.9	CH01
124	2015/05/05	20:49:40.37	39.04631	33.23358	1.8	1.9	ML	1	1.1	91	1.29	4.5	CH01
125	2015/05/05	21:02:38.73	39.0495	33.23849	1.9	1.9	ML	349	1.14	79	1.27	4.5	CH01

5.2. Analysis of Sub-region B

The cluster residing within the Sub-region B is located south east of the Salt Lake, Anatolia which includes the seismic activity from the south eastern end profile of Salt Lake Fault and Ecemiş Fault with the trend of NE-SW which is perpendicular to SLFZ. 163 earthquakes have been relocated and calibrated using the 1-D velocity model that was especially crafted for the region (Table 5.4 and Figure 5.7).

Table 5.4. The crustal velocity model determined and used in the relocation of earthquakes in the Sub-region B.

Depth to Top Layer (km)	P Velocity (km/s)	S velocity (km/s)
0	5.41	3.3
7	5.925	3.44
12	6.55	3.625
35	7.96	4.625

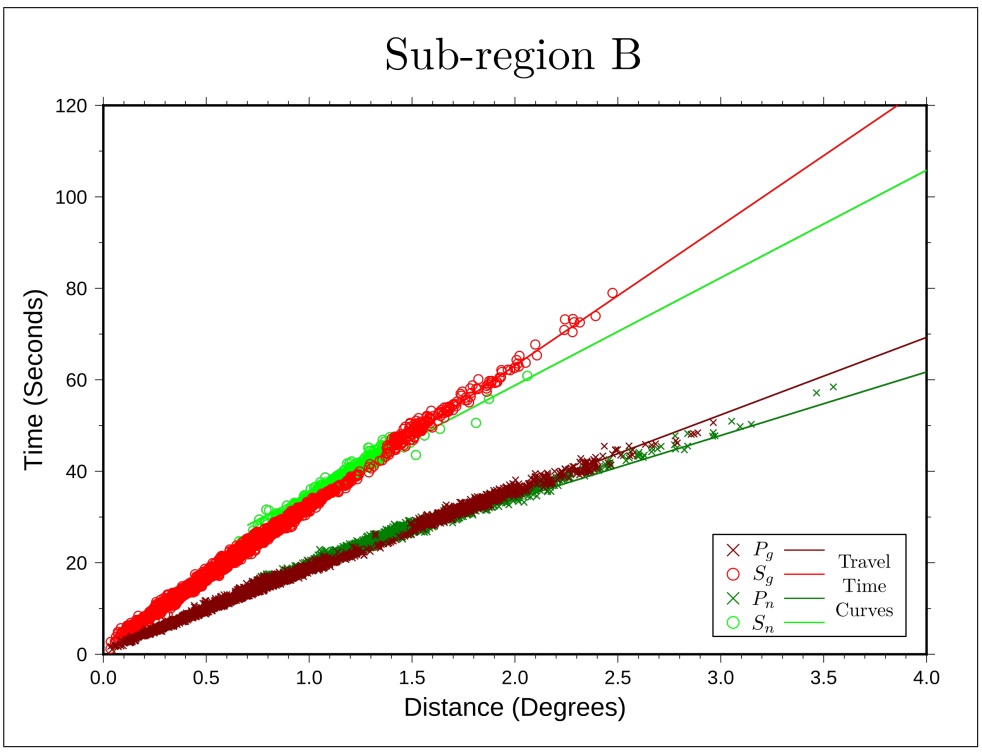

Figure 5.7. Crustal phase arrival times of the earthquakes against the travel time curves of Sub-region B.

A total number of 3176 and 9159 readings have been used to determine hypocentroid and cluster vectors, respectively. Determination of the hypocentroid as well as the application of direct calibration technique have been done by using the 3176 short distance readings ($< 0.7°$) which is shown in Figure 5.8.

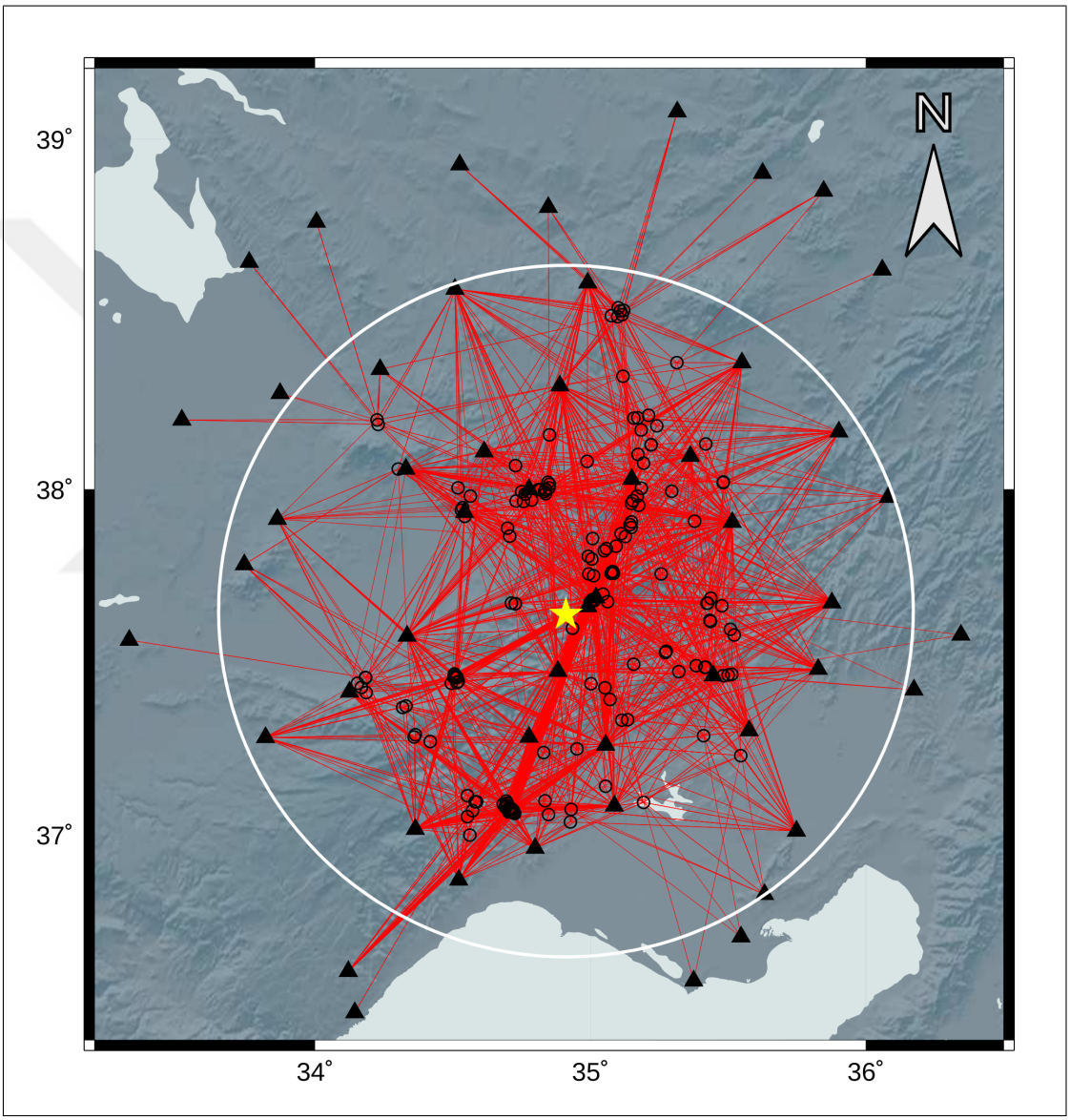

Figure 5.8. Ray paths (red lines) used to locate hypocentroid of the Sub-region B. Triangles are stations and open circles are events used in the direct calibration process. Yellow star denotes the hypocentroid of the cluster and open white circle is centered at the hypocentroid with 1° radius as a scale.

The definition and determination of the "Empirical Path Anomaly" and "Spread" is widely explained in the Section 3.4 and discussed thoroughly in the Section 5.1, "Analysis of Sub-region A".

Empirical path anomaly over spread plots for P_g and S_g phases have been made within the geographic extent of 2° centered at the hypocentroid for each station having 2 or more station phase readings for the events occurred in the Sub-region B.

Map of empirical path anomaly over spread for the P_g phase has been shown in Figure 5.9. According to the map, empirical path anomaly and spread estimations seems coherent within the 1° radius circle with some exceptions. First exception is observed at the same location as the Sub-region A, where a probable slower velocity zone situated ∼40 kilometers away from the southern shores of Salt Lake, near the SULT and AT52 stations. Second exception have similarities with the former but located in the Adana basin. A probable slower structure than average also observed on the stations CEYT and AT50 which are located south-east from the hypocentroid. These stations have the average estimated spread of +0.76 seconds and the residuals are about +0.6 seconds which obtained from the total number of 101 P_g phase observations. Third and final exception is the low negative residuals observed on few stations near the hypocentroid, however, due to the small size they found to be negligible.

Map of empirical path anomaly over spread for the S_g phase has been shown in Figure 5.10. Observations done for the empirical path anomalies of P_g station phases from the Figure 5.9 also correlates with Figure 5.10. Therefore, same conclusion about the slower velocity structure can also be made for the S_g case, concerning the southern part of Salt Lake and Adana basin.

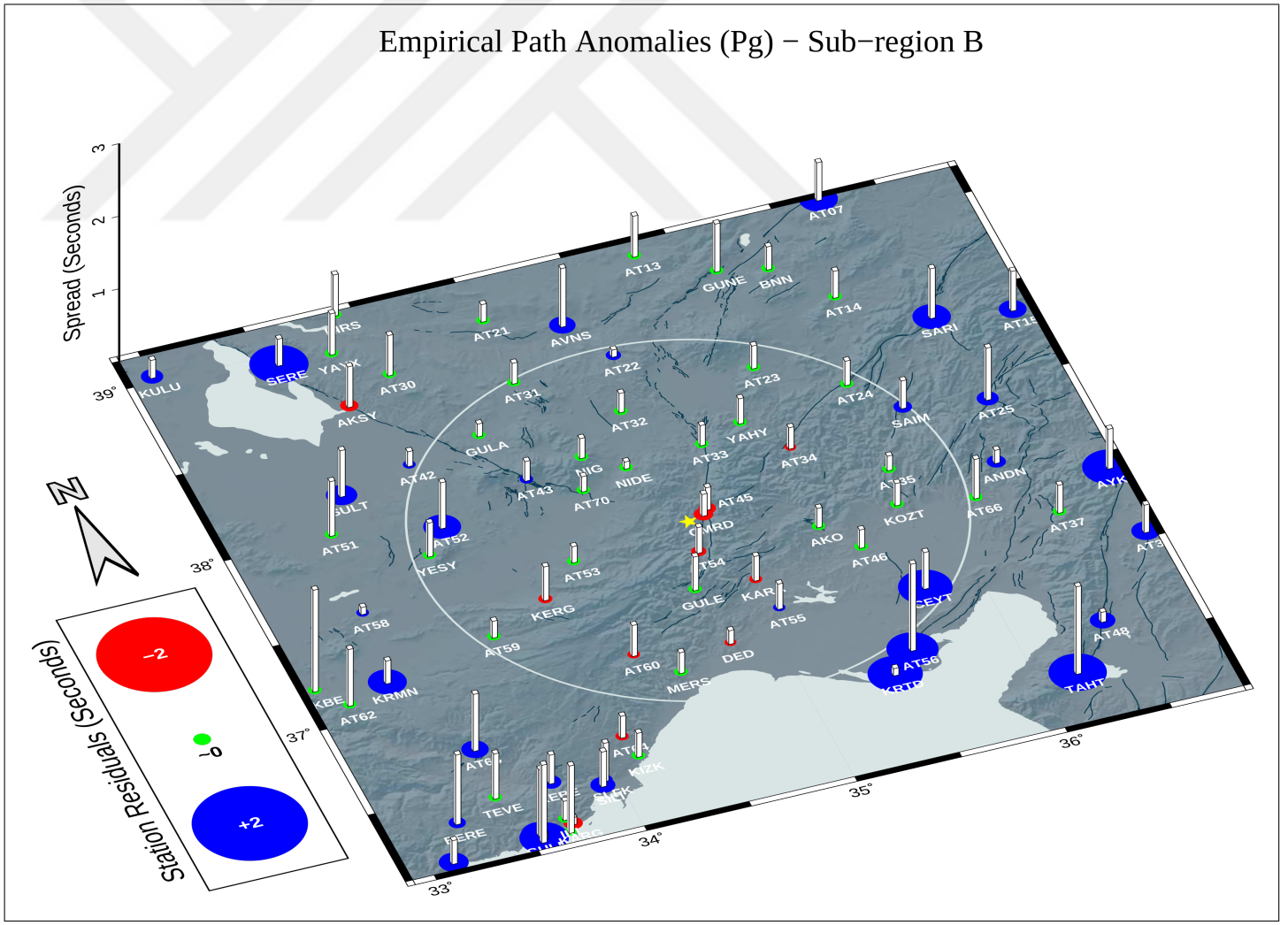

Figure 5.9. Map of empirical path anomaly over spread for the observed P_g station phases for the earthquakes occurred in the Sub-region B. Yellow star denotes the hypocentroid.

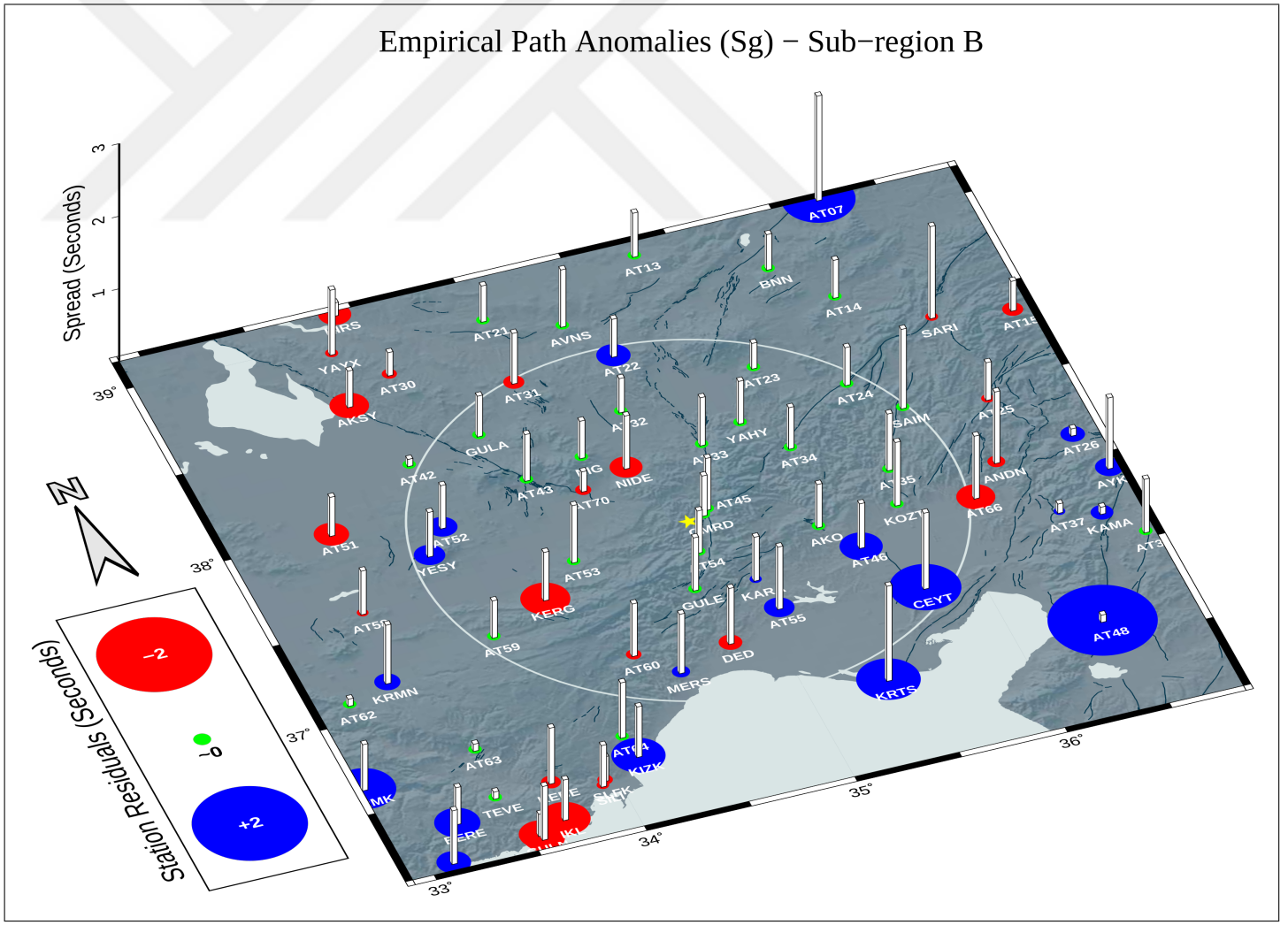

Figure 5.10. Map of empirical path anomaly over spread for the observed S_g station phases for the earthquakes occurred in the Sub-region B. Yellow star denotes the hypocentroid.

Magnitudes reported by ISC and CD-CAT networks for the events relocated in the Sub-region B range from local magnitude (ML) of 1.3 and 3.6. Average of the azimuthal gap for determining cluster vectors is found to be 44.5 degrees. Error ellipses with 90% confidence representing the uncertainties in the location of each event have been estimated, thus, larger semi-axes of the error ellipses observed to vary between 0.6 and 2.4 kilometers. Furthermore, event with the lowest estimated uncertainty (Event #43) has the minor and major semi-axes length of 0.6 km and 0.6 km respectively. The area of the error ellipse of this event is 1.3 km^2. Event with the highest uncertainty (Event #4) has the minor and major semi-axes length of 1.3 km and 1.6 km respectively. The area of the error ellipse of this event is 7.1 km^2.

Results of the 2 events out of 163 have been removed from the final catalogue due to connectivity issues with the cluster.

The resulting catalogue constitutes calibrated locations of 161 events. Focal depths of these events are constrained and average depth of the cluster determined as 5.4 kilometers. Focal depth of 80 earthquakes have been determined by using the near distance readings ($< 0.2°$) with the estimated error of $\sim$2 kilometers. Moreover, focal depths of 41 events have been determined by using the local distance readings with the estimated error of $\sim$4 kilometers. The rest of the 63 events have been fixed to the average depth of the cluster (Figure 5.11). The amount of earthquakes fixed to average depth of the cluster rather large in the Sub-region B compared to Sub-region A. Most obvious reason is the tendency of depths of events in Sub-region B being consistent. Majority of the estimated depths fluctuate with the value of $\pm$3 from the median depth of 6.5 kilometers which results in coherent residuals of phase arrival times used for determining depths even with the fixed depth.

Map of the relocation results along with the depth cross-section for the Sub-region B is shown in the Figure 5.11. Statistics of each relocated and calibrated event is listed in the Table 5.5.

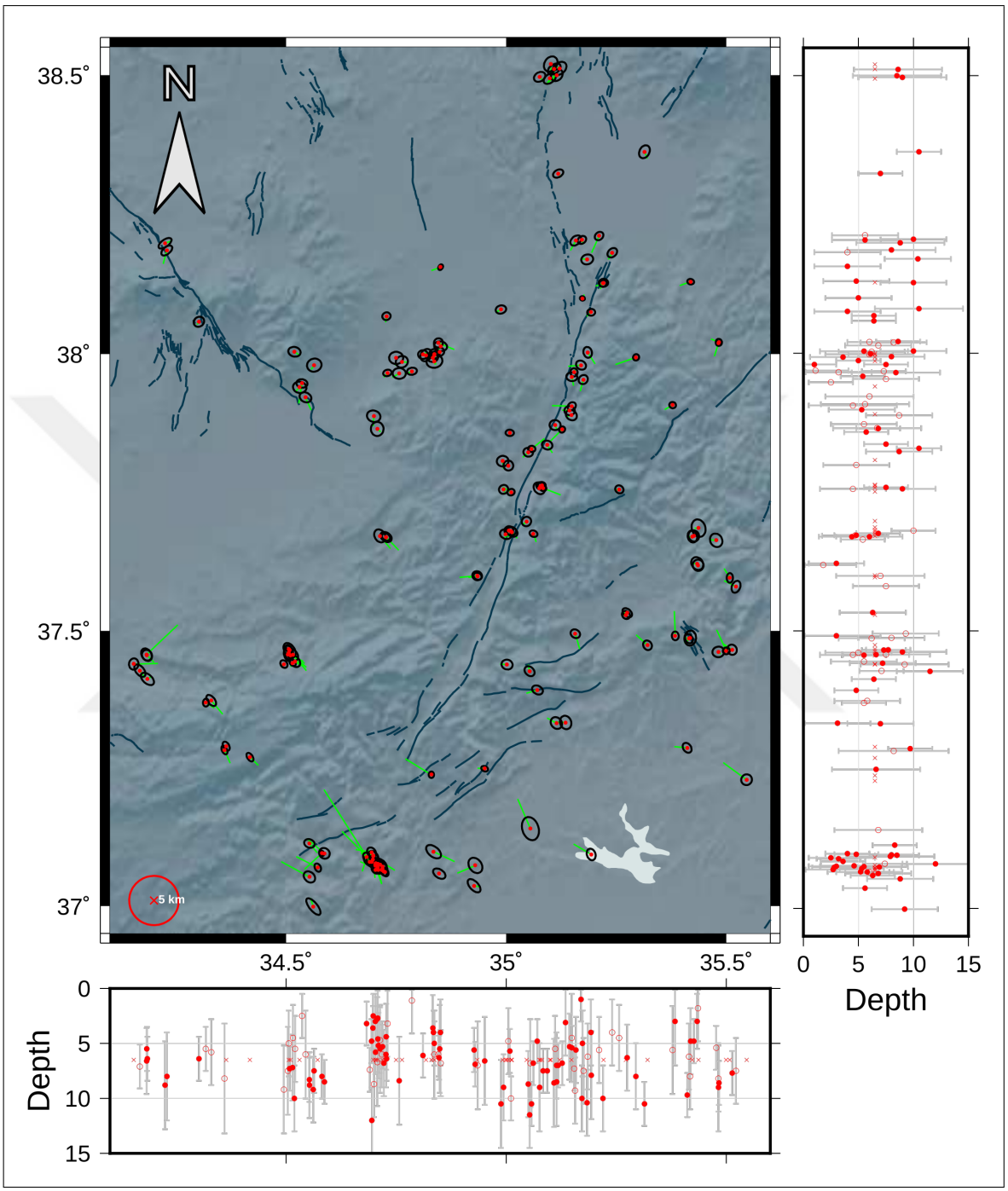

Figure 5.11. Epicenters and depths of earthquakes relocated in the Sub-region B. Map: Red dots are locations and ellipses are for relative location with 90% confidence. Green lines shows the change from the initial single-event location. Open red circle of 5 km radius is shown as a scale. Cross-section: Closed and open red circles are depths determined by near and local distance readings, respectively. Fixed depths marked with an "x". Gray bars are estimates of error on depths.

Table 5.5. Statistics of the earthquakes relocated and calibrated within the Sub-region B. Origin time is given in GMT. Parameters of 90% confidence ellipses are defined as following: AZ1 and AZ2 shows the azimuths of elliptical semi-axes, and, L1 and L2 represents the corresponding lenghts of semi-axes. Area of the confidence ellipses are given in the "Area (km^2)" column. Accuracy codes are defined in the last column. Classification has been done using the procedures explained in Section 3.6.

Event Number	Date	Time	Latitude	Longitude	Depth (km)	Magnitude	Type	AZ1	L1	AZ2	L2	Area (km^2)	GCNU Code
1	2013/06/01	14:41:03.52	37.94748	34.53627	2.5	2.9	ML	10	0.95	100	1.18	3.5	CH01
2	2013/06/01	16:00:37.78	37.09202	34.69822	6.5	2.9	ML	54	0.83	144	1.12	2.9	CT01
3	2013/06/05	15:56:31.49	37.99757	34.81788	6.5	1.9	ML	303	1.11	33	1.38	4.8	CT01
4	2013/06/11	08:56:15.36	37.9868	34.83673	5	2	ML	348	1.38	78	1.65	7.1	CH02
5	2013/06/11	15:58:18.64	37.08475	34.69718	3.6	2.9	ML	62	0.74	152	0.87	2	CH01
6	2013/06/13	01:26:17.81	37.68061	35.01095	10	1.6	ML	15	0.95	105	1.15	3.4	CH01
7	2013/06/15	10:29:10.40	37.09118	34.698	2.5	2.3	ML	44	0.93	134	1.26	3.7	CH01
8	2013/06/19	11:30:57.48	38.02028	34.84576	6	2.3	ML	298	0.98	28	1.03	3.2	CH01
9	2013/06/26	07:54:36.37	37.28775	35.41132	9.7	2.3	ML	55	0.9	145	1.18	3.3	CH01
10	2013/06/26	13:38:31.57	37.88811	34.69947	8.7	2	ML	18	1.21	108	1.43	5.5	CH01
11	2013/07/03	12:57:21.43	37.08052	34.68995	7.4	2.2	ML	37	0.9	127	1.4	3.9	CH01
12	2013/07/15	13:31:27.21	37.09884	34.83465	4	1.9	ML	39	1.11	129	1.81	6.3	CH02
13	2013/07/16	16:19:12.75	37.07685	34.70849	4.6	2.4	ML	50	1.05	140	1.32	4.4	CH01
14	2013/07/22	16:06:48.95	38.20391	35.15833	5.6	1.9	ML	320	0.94	50	1.31	3.9	CH01
15	2013/08/01	12:57:55.80	37.99976	34.83674	6.5	1.8	ML	21	1.07	111	1.12	3.8	CT01
16	2013/08/05	12:41:17.67	37.08041	34.69475	12	2.8	ML	55	0.98	145	1.39	4.3	CH01
17	2013/08/11	13:57:50.27	37.62152	35.43382	3	2	ML	55	1.19	145	1.44	5.4	CH01
18	2013/08/15	23:28:35.21	37.75795	35.07518	6.5	1.4	ML	51	1.1	141	1.35	4.7	CT01
19	2013/08/18	07:26:54.85	38.20528	35.17216	10	1.9	ML	320	0.83	50	1.01	2.7	CH01
20	2013/08/21	15:04:23.00	37.09763	34.69419	4.8	2.7	ML	54	0.93	144	1.12	3.3	CH01
21	2013/08/22	22:07:43.84	37.87216	35.1112	5.5	1.5	ML	7	1.09	97	1.19	4.1	CH01
22	2013/08/24	22:18:53.01	37.52869	35.2719	6.5	2.7	ML	49	0.86	139	0.98	2.6	CT01
23	2013/08/25	13:19:53.38	37.49514	35.15651	9.3	2.4	ML	34	0.93	124	1.09	3.2	CH01
24	2013/08/29	11:44:45.80	38.014	34.85113	6.8	1.9	ML	10	1.05	100	1.38	4.6	CH01

Event Number	Date	Time	Latitude	Longitude	Depth (km)	Magnitude	Type	AZ1	L1	AZ2	L2	Area (km^2)	GCNU Code
25	2013/09/05	20:50:33.12	37.67482	34.99864	6.5	1.7	ML	22	1.02	112	1.26	4.1	CT01
26	2013/09/05	23:23:57.55	38.32368	35.11799	7	1.6	ML	331	0.84	61	1.17	3.1	CH01
27	2013/09/07	20:41:17.97	37.291	34.36395	6.5	1.9	ML	62	0.74	152	1.08	2.5	CT01
28	2013/09/10	01:49:13.81	38.12762	35.22099	6.5	2	ML	358	0.91	88	1.02	2.9	CT01
29	2013/09/13	11:34:56.23	37.6695	34.72688	6	2	ML	36	0.97	126	1.32	4	CH01
30	2013/09/17	09:20:27.42	37.98593	34.76343	6.5	2	ML	329	1.21	59	1.31	5	CT01
31	2013/09/19	15:08:39.00	37.96875	34.78568	1.1	2.2	ML	350	0.83	80	1.08	2.8	CH01
32	2013/09/21	07:07:58.54	38.21248	35.21111	5.6	2.1	ML	319	0.86	49	1.03	2.8	CH01
33	2013/09/25	03:39:02.57	37.59899	34.93509	7	2.8	ML	29	0.8	119	0.95	2.4	CH01
34	2013/09/25	06:44:59.00	38.49683	35.07601	9	1.9	ML	328	1	58	1.28	4	CH01
35	2013/09/29	12:09:42.70	37.53304	35.27465	6.3	2.2	ML	42	0.85	132	1.19	3.2	CH01
36	2013/10/01	00:26:32.94	38.36274	35.3141	10.5	1.5	ML	297	1.07	27	1.43	4.8	CH01
37	2013/10/11	12:09:15.45	37.08948	34.68297	3.2	2.6	ML	65	0.79	155	1.04	2.6	CH01
38	2013/10/24	11:44:07.88	37.9403	34.53056	6.5	2.4	ML	11	1.21	101	1.41	5.4	CT01
39	2013/10/30	15:34:42.57	37.66954	34.72723	4.4	2.2	ML	37	0.8	127	0.98	2.5	CH01
40	2013/10/31	02:38:16.08	37.67561	35.06157	6.8	2.3	ML	21	0.76	111	0.92	2.2	CH01
41	2013/10/31	09:04:57.45	37.99917	34.81101	6.1	2	ML	3	0.97	93	1.07	3.3	CH01
42	2013/10/31	13:42:38.57	37.413	34.18496	6.4	2.3	ML	42	1	132	1.63	5.1	CH02
43	2013/11/01	01:27:18.85	38.09963	35.17317	5	3.6	ML	19	0.62	109	0.67	1.3	CH01
44	2013/11/01	03:55:11.48	37.27096	34.41771	6.5	2.2	ML	57	0.7	147	1.07	2.3	CT01
45	2013/11/04	23:26:48.53	37.6786	35.01289	6.5	1.7	ML	30	0.96	120	1.27	3.8	CT01
46	2013/11/09	17:02:08.30	37.76151	35.07768	6.5	1.9	ML	24	0.85	114	0.99	2.6	CT01
47	2013/11/21	18:30:37.94	37.28371	34.3601	8.2	2.1	ML	67	0.67	157	1.03	2.2	CH01
48	2013/11/29	13:50:30.44	37.06212	34.72477	6.5	2.9	ML	65	0.74	155	1.03	2.4	CT01
49	2013/11/30	09:39:32.49	38.1818	35.24057	4	1.8	ML	317	0.91	47	1.16	3.3	CH01
50	2013/11/30	14:56:31.26	37.6717	34.71335	4.7	1.8	ML	60	1.13	150	1.44	5.1	CH01
51	2013/12/02	02:36:16.23	37.09379	35.19323	7.9	2.1	ML	71	0.96	161	1.28	3.9	CH01
52	2013/12/02	11:45:48.34	37.92226	34.54411	6	2.3	ML	27	1.05	117	1.3	4.3	CH01
53	2013/12/03	13:30:26.05	37.07355	34.70297	6.5	2.7	ML	87	0.92	177	1.11	3.2	CT01
54	2013/12/10	14:31:20.36	37.86522	34.70738	6.7	2	ML	270	1.34	0	1.48	6.2	CH01

Event Number	Date	Time	Latitude	Longitude	Depth (km)	Magnitude	Type	AZ1	L1	AZ2	L2	Area (km^2)	GCNU Code
55	2013/12/10	16:41:26.58	37.85798	35.00821	5.7	1.9	ML	3	0.76	93	0.94	2.2	CH01
56	2013/12/11	20:52:39.45	38.15648	34.85054	4	2.1	ML	301	0.61	31	0.75	1.4	CH01
57	2013/12/13	11:02:08.89	37.33276	35.11434	7	2.2	ML	50	1.14	140	1.33	4.8	CH01
58	2013/12/14	10:55:33.37	37.96574	34.73045	3.2	2.1	ML	343	0.77	73	0.95	2.3	CH01
59	2013/12/17	14:20:40.16	37.67209	35.42632	4.8	1.8	ML	63	1.13	153	1.23	4.4	CH01
60	2013/12/24	13:29:21.05	37.97969	34.56352	7.5	1.9	ML	342	1.37	72	1.52	6.6	CH02
61	2013/12/25	01:09:32.21	37.59644	35.50761	6.5	2.3	ML	90	0.76	180	1.07	2.5	CT01
62	2013/12/25	13:24:50.96	37.0682	34.71893	6.5	2.7	ML	54	0.64	144	0.81	1.6	CT01
63	2013/12/28	18:36:57.73	37.46575	35.51336	7.7	2.4	ML	67	1.04	157	1.14	3.7	CH01
64	2013/12/31	11:47:32.38	37.33362	35.13477	3.1	1.9	ML	70	1.2	160	1.45	5.4	CH01
65	2014/01/04	10:37:37.00	37.99311	34.83331	3.6	1.9	ML	354	0.91	84	1.13	3.2	CH01
66	2014/01/07	13:16:30.02	37.06998	34.70817	2.7	2.5	ML	55	0.76	145	0.97	2.3	CH01
67	2014/01/09	05:08:32.51	37.97952	35.16985	1	2	ML	34	0.96	124	1.14	3.4	CH01
68	2014/01/12	05:55:37.12	38.07536	35.19252	4	1.7	ML	357	0.81	87	0.91	2.3	CH01
69	2014/01/16	09:57:39.98	38.52006	35.10143	6.5	1.8	ML	303	1.3	33	1.67	6.8	CT02
70	2014/01/20	15:01:30.88	37.06578	34.7032	5.8	2	ML	46	0.76	136	1.01	2.4	CH01
71	2014/01/22	11:30:58.17	37.06582	34.70965	5.2	2.3	ML	52	0.81	142	0.97	2.5	CH01
72	2014/01/24	13:54:55.55	37.07401	34.70656	2.8	2.8	ML	59	0.74	149	0.88	2.1	CH01
73	2014/02/03	03:37:08.20	38.08023	34.9882	10.5	2.1	ML	345	0.92	75	1.15	3.3	CH01
74	2014/02/05	10:44:22.59	38.49981	35.11455	8.5	1.8	ML	314	1.1	44	1.37	4.7	CH01
75	2014/02/07	13:54:46.21	37.66437	35.47704	5.4	1.9	ML	62	1.27	152	1.47	5.8	CH01
76	2014/02/07	14:56:24.04	37.06288	34.72202	6.8	2.6	ML	67	0.76	157	1	2.4	CH01
77	2014/02/09	07:47:39.46	37.7556	35.25651	4.5	1.8	ML	39	0.88	129	0.98	2.7	CH01
78	2014/02/09	09:49:22.22	37.61868	35.43572	1.8	1.6	ML	73	1.16	163	1.23	4.5	CH01
79	2014/02/18	13:45:40.85	37.06555	34.71761	6	2.8	ML	60	0.68	150	0.84	1.8	CH01
80	2014/02/18	23:26:34.27	38.00401	34.51891	10	1.5	ML	14	1.05	104	1.32	4.4	CH01
81	2014/02/21	16:27:28.35	37.67063	35.42252	6.5	1.8	ML	76	1.04	166	1.3	4.2	CT01
82	2014/02/22	10:13:35.42	37.07537	34.71369	5.5	2.1	ML	42	1.11	132	1.59	5.6	CH02
83	2014/02/24	13:48:21.22	38.00363	34.849	5.5	2.1	ML	339	0.93	69	0.99	2.9	CH01
84	2014/02/25	11:54:47.32	37.39272	35.07062	4.8	1.5	ML	28	0.95	118	1.23	3.7	CH01

Event Number	Date	Time	Latitude	Longitude	Depth (km)	Magnitude	Type	AZ1	L1	AZ2	L2	Area (km^2)	GCNU Code
85	2014/02/26	22:50:38.42	37.75835	35.08372	7.5	2	ML	16	0.72	106	0.78	1.8	CH01
86	2014/03/04	07:46:00.15	37.0718	34.71906	5.3	2.4	ML	47	0.8	137	1.32	3.3	CH01
87	2014/03/06	18:56:08.26	38.06763	34.72849	6.4	1.9	ML	337	0.88	67	0.94	2.6	CH01
88	2014/03/15	11:29:25.37	37.07269	34.70781	6.5	1.9	ML	38	0.76	128	0.96	2.3	CT01
89	2014/03/18	10:25:41.86	37.99311	34.74973	6.5	1.8	ML	0	1.31	90	1.47	6	CT01
90	2014/03/19	01:17:07.93	37.95853	35.14905	5.4	1.8	ML	9	0.96	99	1.19	3.6	CH01
91	2014/04/04	13:43:11.34	38.51178	35.12135	6.5	1.9	ML	319	1.18	49	1.63	6	CT02
92	2014/04/20	09:23:11.93	37.07601	34.70285	3	1.8	ML	32	0.98	122	1.3	4	CH01
93	2014/04/23	12:49:24.03	38.49447	35.09899	6.5	1.9	ML	325	0.96	55	1.44	4.4	CT01
94	2014/04/28	15:28:28.69	37.0779	34.70383	6.5	2.1	ML	52	0.86	142	1.15	3.1	CT01
95	2014/05/01	10:06:27.99	37.99791	34.8367	6	1.5	ML	332	0.83	62	0.93	2.4	CH01
96	2014/05/11	12:14:49.80	37.90824	35.37785	5.6	2.6	ML	18	0.76	108	0.81	1.9	CH01
97	2014/05/20	15:52:23.82	37.4864	35.41519	6.2	1.9	ML	64	0.84	154	1.08	2.8	CH01
98	2014/05/21	19:06:44.83	37.42698	35.05328	11.5	1.6	ML	46	0.96	136	1.22	3.7	CH01
99	2014/05/27	00:04:08.08	37.23942	34.83019	6.5	2.5	ML	271	0.69	1	0.78	1.7	CT01
100	2014/05/28	00:38:17.57	37.75589	34.99394	9	1.7	ML	324	0.98	54	1.03	3.2	CH01
101	2014/06/09	07:55:04.71	37.07041	34.57186	6.5	2.5	ML	64	0.73	154	0.99	2.3	CT01
102	2014/06/15	09:21:35.04	38.51101	35.10859	8.6	1.9	ML	325	0.98	55	1.49	4.6	CH01
103	2014/06/16	10:45:56.35	37.47435	35.32104	6.5	2.1	ML	61	0.94	151	1.1	3.2	CT01
104	2014/06/17	02:45:21.90	37.79868	35.00484	4.8	1.9	ML	66	1.06	156	1.09	3.6	CH01
105	2014/06/19	12:54:18.75	37.89019	35.14817	6.5	2	ML	37	1.06	127	1.24	4.1	CT01
106	2014/06/29	20:45:18.42	37.68169	35.00589	6.5	1.9	ML	334	0.94	64	0.98	2.9	CT01
107	2014/06/29	23:11:25.82	38.01948	35.4822	8.2	2.6	ML	51	0.65	141	0.66	1.3	CH01
108	2014/07/05	15:22:23.57	37.4404	34.15406	6.5	2	ML	277	1.04	7	1.22	4	CT01
109	2014/07/24	14:03:30.37	37.45604	34.18372	5.5	2.1	ML	58	1.07	148	1.19	4	CH01
110	2014/07/25	02:27:00.44	38.02121	35.4832	8.6	2.6	ML	80	0.76	170	0.82	2	CH01
111	2014/08/01	09:13:37.80	37.03664	34.9272	5.6	1.6	ML	47	0.97	137	1.71	5.2	CH02
112	2014/08/14	12:24:32.29	38.00258	35.18513	6.2	2.2	ML	76	0.94	166	1.18	3.5	CH01
113	2014/08/22	09:58:23.91	37.43925	35.00151	6.5	2	ML	17	1.08	107	1.21	4.1	CT01
114	2014/09/03	13:33:23.35	37.99389	35.2946	8	2.5	ML	296	0.74	26	0.79	1.8	CH01

Event Number	Date	Time	Latitude	Longitude	Depth (km)	Magnitude	Type	AZ1	L1	AZ2	L2	Area (km^2)	GCNU Code
115	2014/09/03	22:06:31.05	37.59993	34.93422	6.5	2	ML	26	0.99	116	1.08	3.4	CT01
116	2014/09/06	00:14:27.01	37.37023	34.31752	5.5	2.2	ML	274	0.74	4	0.91	2.1	CH01
117	2014/09/15	13:38:31.50	37.05922	34.84756	6.3	2.1	ML	34	0.96	124	1.46	4.4	CH01
118	2014/09/17	23:52:04.92	37.80746	34.99203	6.5	1.8	ML	350	1.15	80	1.24	4.5	CT01
119	2014/10/06	07:47:54.08	37.89822	35.1438	5.3	1.9	ML	5	1	95	1.13	3.5	CH01
120	2014/10/10	22:07:53.81	37.46191	35.48208	9	1.5	ML	352	1.15	82	1.28	4.6	CH01
121	2014/10/10	22:40:36.02	37.46376	35.4995	6.5	2.3	ML	329	0.82	59	0.83	2.1	CT01
122	2014/10/19	06:59:57.92	37.05325	34.55321	8.8	2.4	ML	44	1.08	134	1.36	4.6	CH01
123	2014/10/22	01:29:34.41	37.76314	35.08131	6.5	2	ML	15	0.83	105	0.88	2.3	CT01
124	2014/10/25	01:32:56.36	38.12716	35.21963	10	1.8	ML	329	0.79	59	0.87	2.2	CH01
125	2014/11/02	18:33:04.67	37.9059	35.14887	4.5	2.2	ML	316	0.84	46	1	2.6	CH01
126	2014/11/12	14:38:09.39	37.45717	34.18324	6.6	2.5	ML	60	1.06	150	1.43	4.7	CH01
127	2014/11/16	02:48:09.84	37.75083	35.01141	6.5	1.9	ML	334	0.78	64	0.86	2.1	CT01
128	2014/12/04	05:00:41.19	37.69773	35.04642	6.5	2.1	ML	310	1.01	40	1.06	3.4	CT01
129	2014/12/06	17:56:16.40	37.8643	35.12718	6.8	2.2	ML	303	0.72	33	0.78	1.8	CH01
130	2014/12/07	09:19:53.38	38.12982	35.41888	4.8	2.3	ML	12	0.7	102	0.81	1.8	CH01
131	2014/12/24	09:33:27.45	37.58044	35.522	7.5	2.2	ML	292	0.94	22	1.33	3.9	CH01
132	2014/12/30	16:28:50.23	37.48734	35.41765	8	2	ML	277	1.24	7	1.58	6.2	CH02
133	2015/01/16	22:43:51.12	37.37395	34.33017	5.8	1.9	ML	52	0.83	142	1.38	3.6	CH01
134	2015/01/27	10:52:01.95	37.9652	34.75706	8.4	1.7	ML	2	1.17	92	1.38	5.1	CH01
135	2015/02/03	19:15:17.75	38.16981	35.18367	10.4	1.8	ML	345	1.07	75	1.27	4.3	CH01
136	2015/02/04	17:27:52.77	38.19891	34.22508	8.8	1.7	ML	324	0.83	54	1.57	4.1	CH02
137	2015/02/04	18:58:02.90	38.18612	34.22946	8	1.7	ML	319	0.83	49	1.36	3.5	CH01
138	2015/02/05	10:45:17.81	37.42786	34.16761	7.1	2.1	ML	50	0.94	140	1.52	4.5	CH02
139	2015/02/21	22:41:13.84	37.45577	34.51019	6.5	2.4	ML	45	0.67	135	0.87	1.8	CT01
140	2015/02/23	02:43:07.35	37.49109	35.3836	3	1.6	ML	87	0.82	177	0.98	2.5	CH01
141	2015/02/23	08:37:44.49	37.83631	35.09317	7.5	2	ML	19	0.98	109	1.15	3.5	CH01
142	2015/02/24	14:57:10.30	37.1413	35.05479	6.8	2.1	ML	73	1.69	163	2.44	3	CH02
143	2015/02/26	05:32:32.42	37.25043	34.95115	6.6	2.5	ML	24	0.68	114	0.85	1.8	CH01
144	2015/02/28	00:23:45.89	36.99874	34.56167	9.2	2.1	ML	51	0.92	141	2.1	6.1	CH02

Event Number	Date	Time	Latitude	Longitude	Depth (km)	Magnitude	Type	AZ1	L1	AZ2	L2	Area (km^2)	GCNU Code
145	2015/02/28	22:03:41.38	37.4672	34.50607	6.5	3	ML	49	0.7	139	0.89	1.9	CT01
146	2015/02/28	22:26:19.31	37.45677	34.51567	4.5	1.9	ML	56	0.93	146	1.38	4.1	CH01
147	2015/02/28	22:29:27.85	37.4417	34.5146	7.2	2.9	ML	45	0.68	135	0.84	1.8	CH01
148	2015/03/01	01:36:00.90	37.46529	34.50801	7.3	1.8	ML	57	1.1	147	1.68	5.8	CH02
149	2015/03/04	03:18:49.93	37.46067	34.50616	5	1.9	ML	76	0.98	166	1.57	4.8	CH02
150	2015/03/07	06:59:54.75	37.96741	35.15446	7.3	2	ML	88	0.84	178	0.94	2.5	CH01
151	2015/03/10	02:18:28.35	37.44472	34.52038	5.5	1.9	ML	53	1	143	1.36	4.3	CH01
152	2015/03/21	18:09:35.37	37.95369	35.17544	7.5	1.9	ML	316	0.96	46	1.06	3.2	CH01
153	2015/03/26	21:42:53.55	37.45739	34.50397	7.5	2.1	ML	73	0.86	163	1.38	3.7	CH01
154	2015/03/29	15:16:04.45	37.22972	35.5463	6.5	2.2	ML	306	1.15	36	1.19	4.3	CT01
155	2015/04/05	00:52:28.83	37.82877	35.05759	10.5	1.8	ML	9	0.77	99	0.85	2.1	CH01
156	2015/04/05	22:21:52.66	37.82284	35.05	8.7	1.6	ML	20	0.97	110	1.06	3.2	CH01
157	2015/04/06	04:35:45.04	37.09648	34.58143	8	2.7	ML	55	0.64	145	0.73	1.5	CH01
158	2015/04/06	22:55:21.90	37.09578	34.58708	8.5	1.3	ML	47	1.1	137	1.22	4.2	CH01
159	2015/04/13	22:55:08.91	37.11403	34.5529	8.3	1.4	ML	23	0.95	113	1.17	3.5	CH01
160	2015/05/05	11:27:57.35	38.05811	34.30207	6.4	2.2	ML	322	1.05	52	1.18	3.9	CH01
161	2015/05/06	09:19:00.27	37.43957	34.49504	9.2	2.1	ML	52	0.77	142	0.94	2.3	CH01

6. DISCUSSION

In an effort to assess and evaluate the link between seismic activity and tectonic properties of the Salt Lake Region, Anatolia, selected set of well-recorded earthquakes (Section 4.1) occurred within the study area were relocated and calibrated using the mloc technique based on HDC method. The Central Anatolian Region lacks comprehensive earthquake location studies and location solutions made by the seismic monitoring centers are relatively inaccurate due to insufficient seismic stations. Hence, strong emphasis on assessing the uncertainties in the location solutions in this study is solely intended for providing results that will be treated as a reference for the future earthquake location, probabilistic seismic hazard analysis (PSHA) or other comparative studies that will be conducted in the Salt Lake Region, Anatolia.

In the study, calibrated locations of the seismic events took place between mid 2013 to mid 2015 were demonstrated (Figure 5.6 and 5.11). According to the maps of relocation results, depth cross-sections and other empirical evidences (Section 5), following notable findings have been made: Slower velocity and deeper than average seismic zone residing south of Salt Lake in the Eskil, Aksaray is found and linked with the intrusions that Tavşanlı subduction zone had produced (Figure 2.4 and 6.1). The diapiric salt structure formed beneath Eskil, Aksaray by intrusions is remarked and illustrated in [51]. A recent local seismic tomography study conducted for the Central Anatolian Region [52] is also suggested a slower than average velocity zone for the same spot (Figure 6.2). A deeper than average cluster depth of earthquakes observed in the Salt Lake basin, near the center of SLFZ, Altınkaya (Figure 6.1). It is proposed to stem from the deformation caused by intrusive volcanic rocks situated along Şereflikocahisar to Aksaray (Figure 2.3). A similar occurrence is also observed in Topakkaya, Aksaray along the Salt Lake fault plane where seismic activity were found in the average depth of 8 kilometers (Figure 5.6 and 6.1). Even though SLFZ isn't observed as very active along its path for the given 2 years of time period, same observation cannot be made for northern branch of the EFZ which is displaying perfectly aligned activity to the fault plane. However, southern half of the EFZ lacks earthquake activity which reveals a

seismic gap for the given time period (Figure 5.11 and 6.1). No correlation were found between the poly-genetic volcanoes and the seismic activity that has been relocated and calibrated (Figure 2.5 and 6.1).

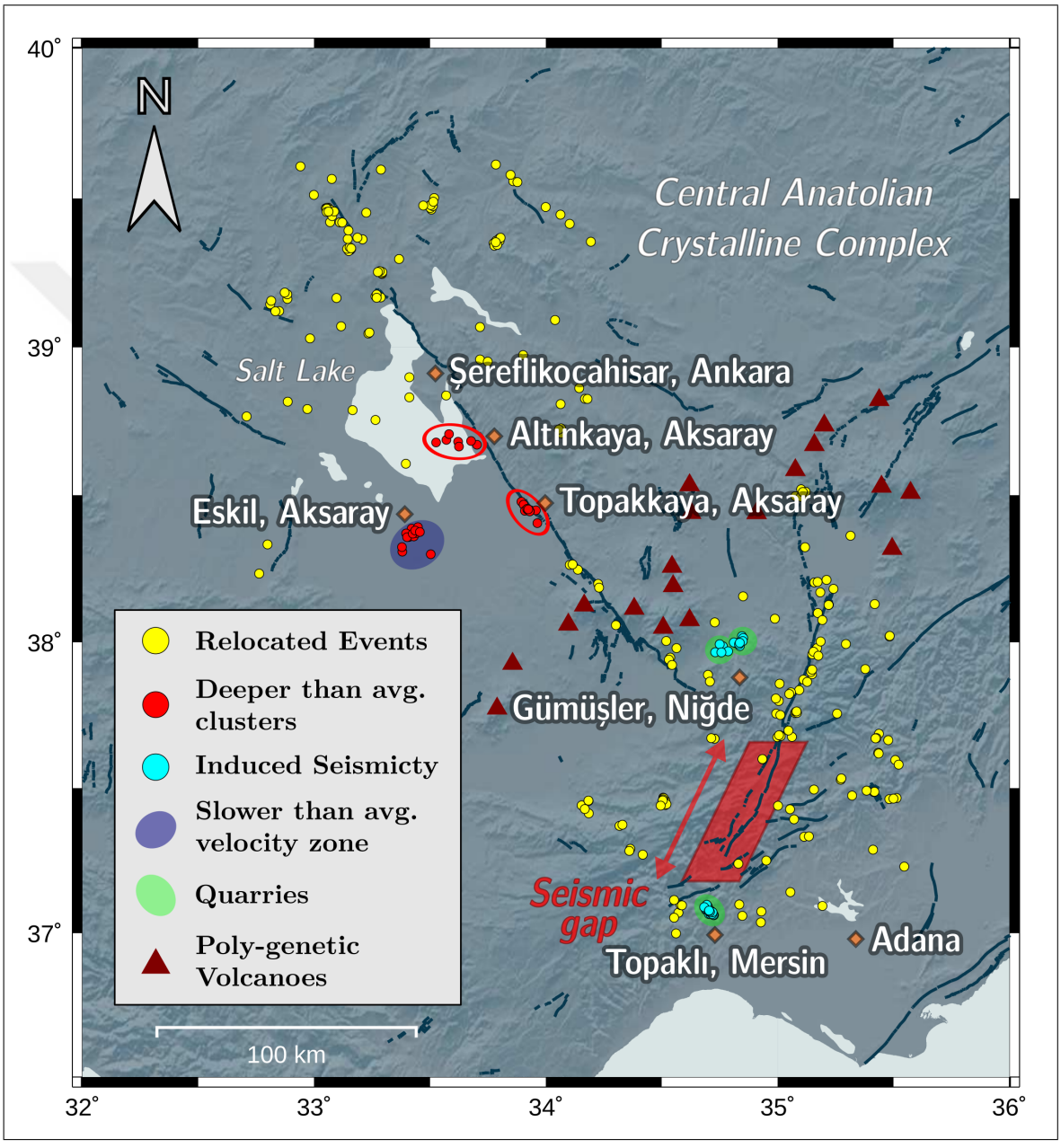

Figure 6.1. The map illustrating notable findings in the study.

The NVC is very rich in metamorphic sediments. They contain significant amount of calsite minerals, hence, several calsite quarries and mines are operated in this region. Mining operations usually include quarry blasts, withdrawal of groundwater and removal of surface material. These type of actions changing the structural integrity

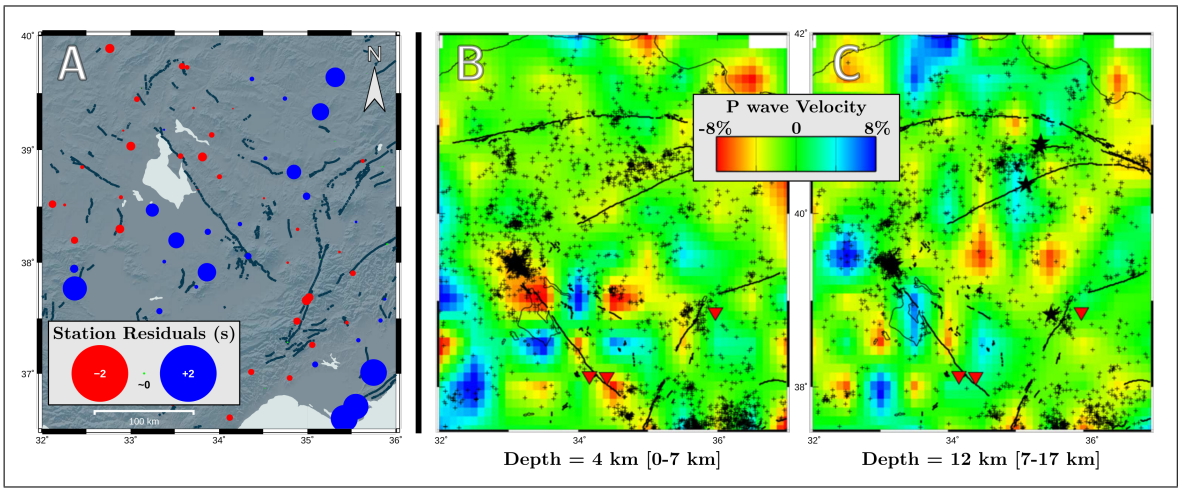

Figure 6.2. A: The map showing the average residuals of the stations, illustrating early (red circles) and late (blue circles) crustal P phase arrivals compared to local velocity models used in the study. B and C: Change of P wave velocity structure (in percent) of the Central Anatolia, varying by depth, modified from [52].

decreases normal stress and increases shear stress, therefore, may lead to triggered or so called induced seismicity in the uppermost part of crust if the region is tectonically active [53–55]. Throughout the depth determination process, depth of various seismic events were solved as very near to the surface level or above. Epicenter of these type of events were checked from the satellite imagery, then according to the results, removed from the cluster or re-investigated. However, there are other cases where clustering is observed around the quarries and no-connections could be made to define those events as quarry blasts. Two clusters were found in Gümüşler, Niğde and one cluster in Topaklı, Mersin suiting to described example (Figure 6.1). Considering the fact that NVP is a very complex and deformed region due to burial and exhumation cycles it went through, the two clusters observed in Niğde are probably the seismic activities induced by the mining activities. However, further investigations should be made by using the methodologies such as [56] or [57] in order comprehend the nature of these events.

Taking the current calibrated relocation solutions into an improved level is possible by using the Bayesloc algorithm. The Bayesloc algorithm allows prior probabilistic

information to be used in its relocation process, including the distribution of hypocentral parameters and error estimations. In the future studies, calibrated location solutions derived from mloc can be used as priors in the Bayesloc algorithm along with the data spanning wider time-range and region, which will be a great advancement over the current relocation results.

7. CONCLUSIONS

Local seismic activity that occurred within the limits of the study area have been relocated and calibrated using the multiple event relocation technique "mloc" which is based on hypocentroidal decomposition (HDC) algorithm. Hypocentral parameters as well as the corresponding uncertainties of the total number of 394 earthquakes have been extensively evaluated and classified with the analyses that have been done for the interest regions Sub-region A and Sub-region B separately (Chapter 5). Reassessed and calibrated multiple event relocation solutions of the earthquakes have significantly improved the initial locations by making use of not only the merged catalog of the CD-CAT network with the International Seismological Centre (ISC), but also the custom 1-D velocity models that have been specifically crafted by fitting these rich arrival time data set (Figure 5.2 and 5.7).

First analysis has been carried out for Sub-region A where the Salt Lake Fault Zone (SLFZ) is located (Section 5.1). Three layered, 1-D crustal velocity model with P and S wave velocities of 5.5 km/s and 3.37 km/s for the top 6 kilometers, 6.0 km/s and 3.47 km/s between 6 to 11 kilometers and lastly 6.5 km/s and 3.6 km/s from 11 kilometers to the Moho, which is at 36 kilometers has been found to suit best for the region (Table 5.2). Average depth of the cluster has been determined as 5.7 kilometers. A total number of 114 earthquakes have been classified as CH01, 3 as CT01 and 8 as CH02 in Sub-region A (Table 5.3). A possible slower velocity zone has been detected in Eskil, Aksaray. Moreover, earthquakes occurred near this region have been observed to strike deeper ($\sim$10 km) than the average cluster depth, indicating the complex diapiric structure Tavşanlı subduction zone and its remnants have been created. Two deeper than average clusters has been found in Altınkaya and Topakkaya, Aksaray is linked with the deformations caused by intrusive volcanic rocks located along SLFZ. No connection could be made between poly-genetic volcanoes and the relocated and calibrated seismic activity for this sub-region (Figure 6.1).

Second and final analysis has been carried out for Sub-region B where the Ecemiş Fault Zone (EFZ) is located (Section 5.2). Three layered, 1-D crustal velocity model with P and S wave velocities of 5.41 km/s and 3.3 km/s for the top 7 kilometers, 5.92 km/s and 3.44 km/s between 7 to 12 kilometers and lastly 6.5 km/s and 3.62 km/s from 12 kilometers to the Moho, which is at 35 kilometers has been found to suit best for the region (Table 5.4). Average depth of the cluster has been determined as 5.4 kilometers. A total number of 108 earthquakes have been classified as CH01, 38 as CT01, 13 as CH02 and 2 as CT02 in Sub-region B (Table 5.5). Northern half of the EFZ was seismically very active and earthquakes which occurred in this region has been found to align to the fault plane properly. Although same observation cannot be made for the southern branch of the fault plane as no activity has been observed for the given period of time. Three calsite quarries have been suspected to induce shallow seismic activity linked with the mining operations since no evidence were found to describe these events as quarry blasts (Figure 6.1). Finally, a slower than average velocity zone has been observed near Adana basin, however, no earthquakes have been relocated near Adana as it is outside the limits of study region.

REFERENCES

1. Celâl, A., Y. Yilmaz *et al.*, "Tethyan evolution of Turkey: a plate tectonic approach", *Tectonophysics*, Vol. 75, No. 3-4, pp. 181193203–190199241, 1981.

2. Reilinger, R., S. McClusky, M. Oral, R. King, M. Toksoz, A. Barka, I. Kinik, O. Lenk and I. Sanli, "Global Positioning System measurements of present-day crustal movements in the Arabia-Africa-Eurasia plate collision zone", *Journal of Geophysical Research: Solid Earth*, Vol. 102, No. B5, pp. 9983–9999, 1997.

3. McClusky, S., S. Balassanian, A. Barka, C. Demir, S. Ergintav, I. Georgiev, O. Gurkan, M. Hamburger, K. Hurst, H. Kahle *et al.*, "Global Positioning System constraints on plate kinematics and dynamics in the eastern Mediterranean and Caucasus", *Journal of Geophysical Research: Solid Earth*, Vol. 105, No. B3, pp. 5695–5719, 2000.

4. Walker, R., E. Bergman, W. Szeliga and E. Fielding, "Insights into the 1968-1997 Dasht-e-Bayaz and Zirkuh earthquake sequences, eastern Iran, from calibrated relocations, InSAR and high-resolution satellite imagery", *Geophysical Journal International*, Vol. 187, No. 3, pp. 1577–1603, 2011.

5. Bergman, E. A. and S. C. Solomon, "Earthquake Swarms on the Mid-Atlantic Ridge: Products of Magmatism or Extensional Tectonics", *Journal of Geophysical Research*, Vol. 95, 1990.

6. Jordan, T. H. and K. A. Sverdrup, "Teleseismic location techniques and their application to earthquake clusters in the south-central Pacific", *Bulletin of the Seismological Society of America*, Vol. 71, No. 4, pp. 1105–1130, 1981.

7. Vanacore, E., T. Taymaz and E. Saygin, "Moho structure of the Anatolian Plate from receiver function analysis", *Geophysical Journal International*, Vol. 193, No. 1, pp. 329–337, 2013.

8. Reilinger, R., S. McClusky, P. Vernant, S. Lawrence, S. Ergintav, R. Cakmak, H. Ozener, F. Kadirov, I. Guliev, R. Stepanyan *et al.*, "GPS constraints on continental deformation in the Africa-Arabia-Eurasia continental collision zone and implications for the dynamics of plate interactions", *Journal of Geophysical Research: Solid Earth*, Vol. 111, No. B5, 2006.

9. Şengör, A., "The North Anatolian transform fault: its age, offset and tectonic significance", *Journal of the Geological Society*, Vol. 136, No. 3, pp. 269–282, 1979.

10. Barka, A. and K. Kadinsky-Cade, "Strike-slip fault geometry in Turkey and its influence on earthquake activity", *Tectonics*, Vol. 7, No. 3, pp. 663–684, 1988.

11. Storetvedt, K. M., *Global wrench tectonics: theory of earth evolution*, Fagbokforlaget, 2003.

12. Bilim, F. and A. Ates, "Identifying block rotations from remanent magnetization effect: Example from northern Central Turkey", *Earth, planets and space*, Vol. 59, No. 1, pp. 33–38, 2007.

13. Büyüksaraç, A., "Investigation into the regional wrench tectonics of inner East Anatolia (Turkey) using potential field data", *Physics of the Earth and Planetary Interiors*, Vol. 160, No. 1, pp. 86–95, 2007.

14. Şengör, A., "Strike-slip faulting and related basin formation in zones of tectonic escape: Turkey as a case study", *Special Publications of SEPM*, 1985.

15. Tan, O., M. C. Tapırdamaz, S. Ergintav, S. İnan, Y. Iravul, R. Saatçılar, B. Tüzel, A. Tarancıoğlu, S. Karakısa, R. F. Kartal *et al.*, "Bala (Ankara) earthquakes: Implications for shallow crustal deformation in central Anatolian section of the Anatolian platelet (Turkey)", *Turkish Journal of Earth Sciences*, Vol. 19, No. 4, pp. 449–471, 2010.

16. Piper, J., O. Tatar, H. Gursoy, F. Koçbulut and B. Mesci, "Paleomagnetic anal-

ysis of neotectonic deformation in the Anatolian accretionary collage, Turkey", *Geological Society of America Special Papers*, Vol. 409, pp. 417–439, 2006.

17. Emre, O., T. Duman, S. Özalp, H. Elmacı, S. Olgun and F. Şaroğlu, *1/1.125.000 Ölçekli Türkiye Diri Fay Haritası*, Maden Tetkik ve Arama Genel Müdürlüğü Özel Yayınlar Serisi, Ankara, Türkiye, 2013, http://www.mta.gov.tr.

18. Schildgen, T. F., C. Yıldırım, D. Cosentino and M. R. Strecker, "Linking slab break-off, Hellenic trench retreat, and uplift of the Central and Eastern Anatolian plateaus", *Earth-Science Reviews*, Vol. 128, pp. 147–168, 2014.

19. Aydin, F., A. K. Schmitt, W. Siebel, M. Sönmez, Y. Ersoy, A. Lermi, K. Dirik and R. Duncan, "Quaternary bimodal volcanism in the Niğde Volcanic Complex (Cappadocia, central Anatolia, Turkey): age, petrogenesis and geodynamic implications", *Contributions to Mineralogy and Petrology*, Vol. 168, No. 5, p. 1078, 2014.

20. Dhont, D., J. Chorowicz, T. Yürür, J.-L. Froger, O. Köse and N. Gündogdu, "Emplacement of volcanic vents and geodynamics of Central Anatolia, Turkey", *Journal of Volcanology and Geothermal Research*, Vol. 85, No. 1, pp. 33–54, 1998.

21. Lefebvre, C. J. C., *The tectonics of the Central Anatolian Crystalline Complex: a structural, metamorphic and paleomagnetic study*, Departement Aardwetenschappen, 2011.

22. Parlak, O., F. Karaoğlan, T. Rızaoğlu, U. Klötzli, F. Koller and Z. Billor, "U–Pb and 40 Ar–39 Ar geochronology of the ophiolites and granitoids from the Tauride belt: implications for the evolution of the Inner Tauride suture", *Journal of Geodynamics*, Vol. 65, pp. 22–37, 2013.

23. Toprak, V. and M. Göncöoğlu, "Tectonic control on the development of the Neogene-Quaternary Central Anatolian Volcanic Province, Turkey", *Geological Journal*, Vol. 28, No. 3-4, pp. 357–369, 1993.

24. Arikan, Y., "The geology and petroleum prospects of the Tuz Gölü Basin", *MTA Bulletin*, Vol. 85, pp. 17–37, 1975.

25. Bozkurt, E., "Neotectonics of Turkey–a synthesis", *Geodinamica acta*, Vol. 14, No. 1-3, pp. 3–30, 2001.

26. Görür, N., F. Oktay, I. Seymen and A. Şengör, "Palaeotectonic evolution of the Tuzgölü basin complex, Central Turkey: sedimentary record of a Neo-Tethyan closure", *Geological Society, London, Special Publications*, Vol. 17, No. 1, pp. 467–482, 1984.

27. Aydemir, A., "Tectonic investigation of Central Anatolia, Turkey, using geophysical data", *Journal of Applied Geophysics*, Vol. 68, No. 3, pp. 321–334, 2009.

28. Koçyiğit, A. and A. Beyhan, "A new intracontinental transcurrent structure: the Central Anatolian Fault Zone, Turkey", *Tectonophysics*, Vol. 284, No. 3, pp. 317–336, 1998.

29. Toprak, V., "Vent distribution and its relation to regional tectonics, Cappadocian Volcanics, Turkey", *Journal of Volcanology and Geothermal Research*, Vol. 85, No. 1, pp. 55–67, 1998.

30. Umhoefer, P. J., D. L. Whitney, C. Teyssier, A. K. Fayon, G. Casale and M. T. Heizler, "Yo-yo tectonics in a wrench zone, Central Anatolian fault zone, Turkey", *Geological Society of America Special Papers*, Vol. 434, pp. 35–57, 2007.

31. Jaffey, N. and A. H. Robertson, "New sedimentological and structural data from the Ecemiş Fault Zone, southern Turkey: implications for its timing and offset and the Cenozoic tectonic escape of Anatolia", *Journal of the Geological Society*, Vol. 158, No. 2, pp. 367–378, 2001.

32. Geiger, L., "Probability method for the determination of earthquake epicenters from the arrival time only", *Bull. St. Louis Univ*, Vol. 8, No. 1, pp. 56–71, 1912.

33. Douglas, A., "Joint epicentre determination", *Nature*, Vol. 215, pp. 47–48, 1967.

34. Kissling, E., "Geotomography with local earthquake data", *Reviews of Geophysics*, Vol. 26, No. 4, pp. 659–698, 1988.

35. Pujol, J., "Joint event location—the JHD technique and applications to data from local seismic networks", *Advances in seismic event location*, pp. 163–204, Springer, 2000.

36. Waldhauser, F. and W. L. Ellsworth, "A double-difference earthquake location algorithm: Method and application to the northern Hayward fault, California", *Bulletin of the Seismological Society of America*, Vol. 90, No. 6, pp. 1353–1368, 2000.

37. Myers, S. C., G. Johannesson and W. Hanley, "A Bayesian hierarchical method for multiple-event seismic location", *Geophysical Journal International*, Vol. 171, No. 3, pp. 1049–1063, 2007.

38. Bergman, E. A., *Multiple Event Relocation at the National Earthquake Information Center*, Tech. rep., Award No. G11AP20016, Golden-Colorado, 2014.

39. Zanjani, A. A., A. Ghods, F. Sobouti, E. Bergman, G. Mortezanejad, K. Priestley, S. Madanipour and M. Rezaeian, "Seismicity in the western coast of the South Caspian Basin and the Talesh Mountains", *Geophysical Journal International*, Vol. 195, No. 2, pp. 799–814, 2013.

40. Croux, C. and P. J. Rousseeuw, *Time-efficient algorithms for two highly robust estimators of scale*, Universitaire Instelling Antwerpen. Department of Mathematics, 1992.

41. Bondár, I., S. C. Myers, E. R. Engdahl and E. A. Bergman, "Epicentre accuracy based on seismic network criteria", *Geophysical Journal International*, Vol. 156, No. 3, pp. 483–496, 2004.

42. Sandvol, E., *Continental Dynamics/Central Anatolian Tectonics: Surface to mantle dynamics during collision to escape*, International Federation of Digital Seismograph Networks, 2013, other/Seismic Network.

43. Centre, I. S., *On-line Bulletin*, Internatl. Seismol. Cent., Thatcham, United Kingdom, 2016, http://www.isc.ac.uk.

44. Kennett, B., E. Engdahl and R. Buland, "Constraints on seismic velocities in the Earth from traveltimes", *Geophysical Journal International*, Vol. 122, No. 1, pp. 108–124, 1995.

45. Wessel, P., W. H. Smith, R. Scharroo, J. Luis and F. Wobbe, "Generic mapping tools: Improved version released", *Eos, Transactions American Geophysical Union*, Vol. 94, No. 45, pp. 409–410, 2013.

46. Wessel, P. and W. H. Smith, "New, improved version of Generic Mapping Tools released", *Eos, Transactions American Geophysical Union*, Vol. 79, No. 47, pp. 579–579, 1998.

47. Wessel, P. and W. H. Smith, "New version of the generic mapping tools", *Eos, Transactions American Geophysical Union*, Vol. 76, No. 33, pp. 329–329, 1995.

48. Wessel, P. and W. H. Smith, "Free software helps map and display data", *Eos, Transactions American Geophysical Union*, Vol. 72, No. 41, pp. 441–446, 1991.

49. Havskov, J. and L. Ottemöller, *Routine data processing in earthquake seismology: with sample data, exercises and software*, Springer Verlag, 2010.

50. Shearer, P. M., *Introduction to Seismology*, Cambridge University Press, 2009.

51. Coskun, B., "Aksaray and Ecemis Faults—Diapiric Salt Relationships: Relevance to the Hydrocarbon Exploration in the Tuz Golu (Salt Lake) Basin, Central Anatolia, Turkey", *Energy sources*, Vol. 26, No. 11, pp. 1005–1022, 2004.

52. Salah, M. K., Ş. Şahin and U. Topatan, "Crustal velocity and Vp/Vs structures beneath central Anatolia from local seismic tomography", *Arabian Journal of Geosciences*, Vol. 7, No. 10, pp. 4101–4118, 2014.

53. Guha, S., "Mining Induced Seismicity", *Induced Earthquakes*, pp. 159–215, Springer, 2000.

54. Gibowicz, S. J. and S. Lasocki, "Seismicity induced by mining: Ten years later", *Advances in geophysics*, Vol. 44, pp. 39–181, 2001.

55. McGarr, A., D. Simpson and L. Seeber, "Case histories of induced and triggered seismicity", *International Geophysics Series*, Vol. 81, No. A, pp. 647–664, 2002.

56. Abdul-Wahed, M. K., M. Al Heib and G. Senfaute, "Mining-induced seismicity: Seismic measurement using multiplet approach and numerical modeling", *International Journal of Coal Geology*, Vol. 66, No. 1, pp. 137–147, 2006.

57. Grigoli, F., S. Cesca, M. Vassallo and T. Dahm, "Automated seismic event location by travel-time stacking: An application to mining induced seismicity", *Seismological Research Letters*, Vol. 84, No. 4, pp. 666–677, 2013.